Eur. Phys. J. C (2011) 71:1721
DOI 10.1140/epjc/s10052-011-1721-3

THE EUROPEAN PHYSICAL JOURNAL C

Regular Article - Experimental Physics

Measurement of the $t\bar{t}$ production cross section in pp collisions at $\sqrt{s} = 7$ TeV using the kinematic properties of events with leptons and jets

The CMS Collaboration*
CERN, 1211 Geneva 23, Switzerland

Received: 7 June 2011 / Revised: 8 July 2011 / Published online: 20 September 2011

Abstract A measurement of the $t\bar{t}$ production cross section in proton-proton collisions at a centre-of-mass energy of 7 TeV has been performed at the LHC with the CMS detector. The analysis uses a data sample corresponding to an integrated luminosity of 36 pb^{-1} and is based on the reconstruction of the final state with one isolated, high transverse-momentum electron or muon and three or more hadronic jets. The kinematic properties of the events are used to separate the $t\bar{t}$ signal from W+jets and QCD multijet background events. The measured cross section is 173^{+39}_{-32} (stat.+syst.) pb, consistent with standard model expectations.

1 Introduction

The top quark occupies a unique position within the standard model. With a mass roughly that of a tungsten atom, it is the only quark heavy enough to decay before forming bound states with other quarks. Its large mass has inspired numerous theoretical models in which the top quark plays a special role in the generation of mass or in the physics of new, undiscovered particles. The top quark often acts as either a direct contributor to new physics or an important background in new-particle searches in these models.

In hadron colliders, top-quark production is dominated by the production of $t\bar{t}$ pairs [1]. At the Tevatron, where the top quark was discovered in 1995 [2, 3], $t\bar{t}$ pairs are predominantly produced through quark-antiquark annihilation. In contrast, the $t\bar{t}$ production mechanism at the Large Hadron Collider (LHC) [4] is expected to be dominated by the gluon fusion process. Measurements of the $t\bar{t}$ cross section at the LHC can provide important tests of our understanding of the top-quark production mechanism and can also be used in searches for new physics.

In the standard model, a top quark decays nearly 100% of the time to a W boson and a b quark. The decay of a $t\bar{t}$ pair is categorized by the decay of the W bosons produced by the pair. Thus the channel in which both W bosons decay to leptons is referred to as the "dilepton" channel, and the channel in which one W decays to leptons and the other to quark jets is the "lepton + jets" channel. The channel in which both W bosons decay to jets is called the "all hadronic" channel. A further categorization of the decays is made by specifying the flavor of the charged lepton(s) produced from the W decays. For the purposes of this paper, the "lepton + jets" channel refers only to decays in which the charged lepton is either an electron or a muon.

The next-to-leading-order (NLO) corrections to the top-quark pair production cross section at hadron colliders have been calculated both with the full top-quark spin dependence [5, 6] and without this dependence [7, 8]. A complete analytic result for the NLO partonic cross section has only been published recently [9]. Approximations of a full next-to-next-to-leading-order (NNLO) calculation have also been obtained by various groups [10–13, and references therein]. The $t\bar{t}$ production cross section at the LHC has been previously measured in the dilepton channel by the Compact Muon Solenoid (CMS) experiment [14] and in the combined dilepton and lepton + jets channels by the ATLAS experiment [15]. These measurements agree with recent NLO and with approximate NNLO calculations.

In this paper we present a measurement of the cross section for $t\bar{t}$ production in proton-proton collisions at $\sqrt{s} = 7$ TeV with the CMS detector, using the electron+jets and muon+jets final states. Although there are two jets from hadronization of the b quarks in these final states, in this analysis no requirement is made on the presence of b jets. Instead, the kinematic properties of the events are used to select the $t\bar{t}$ signal. It is important to measure the $t\bar{t}$ cross section both with and without a requirement on the presence

* e-mail: cms-publication-committee-chair@cern.ch

of b jets, as new physics could contribute differently in each case.

A brief overview of the CMS detector is provided in Sect. 2 of this paper, followed by a discussion of event reconstruction procedures in Sect. 3. The selection criteria applied to the data are described in Sect. 4 and the processes used to simulate signal and background events are described in Sect. 5. Section 6 details the method used to extract a measurement of the $\mathrm{t\bar{t}}$ cross section from the selected events, as well as the calculation of statistical and systematic uncertainties on the result. Section 7 summarizes the result and compares the measurement with recent perturbative QCD calculations.

2 CMS detector

The central feature of the CMS apparatus is a 3.8 T magnetic field produced by a superconducting solenoid of 6 m internal diameter. Within the field volume are the silicon pixel and strip trackers, the crystal electromagnetic calorimeter (ECAL), and the hadron calorimeter (HCAL). The inner tracker measures charged particles within the range $|\eta| < 2.5$, where η indicates detector pseudorapidity. It consists of 1440 silicon pixel and 15 148 silicon strip detector modules and is located within the axial magnetic field. It provides an impact parameter resolution of $\sim$15 μm and a transverse momentum (p_{T}) resolution of $\sim$1.5% for 100 GeV particles. The ECAL consists of nearly 76 000 lead tungstate crystals that provide coverage in pseudorapidity of $|\eta| < 1.48$ in the ECAL barrel region and $1.48 < |\eta| < 3.0$ in the two endcaps. A preshower detector consisting of two planes of silicon sensors interleaved with a total of 3 radiation lengths of lead is located in front of the endcaps. The ECAL energy resolution is 3% or better for the range of electron energies relevant for this analysis.

The HCAL is composed of layers of plastic scintillator within a brass/stainless steel absorber, covering the region $|\eta| < 3.0$. A calorimeter composed of quartz fibers embedded in a steel absorber extends the forward HCAL coverage beyond the solenoid volume, to $|\eta| < 5.0$. In the region $|\eta| < 1.74$, the HCAL cells have widths of 0.087 in both pseudorapidity and azimuth (ϕ). In the (η, ϕ) plane, for $|\eta| < 1.48$, the HCAL cells match the underlying 5×5 ECAL crystal arrays to form calorimeter towers projecting radially outwards from close to the nominal interaction point. At larger values of $|\eta|$, the size of the towers increases, and the matching ECAL arrays contain fewer crystals.

Muons are measured in the pseudorapidity window $|\eta| < 2.4$, with detection planes made of drift tubes, cathode strip chambers, and resistive plate chambers. Matching the muons to the tracks measured in the silicon tracker results in a transverse-momentum resolution between 1% and 5% for p_{T} values up to 1 TeV. A two-tier trigger system selects the most interesting pp collision events for use in physics analyses. A more detailed description of the CMS detector can be found elsewhere [16].

3 Event reconstruction

The reconstruction of electrons [17, 18] uses information from the pixel detector, the silicon strip tracker, and the electromagnetic calorimeter. The amount of material before the ECAL in the CMS detector ranges from 0.4 to 1.6 radiation lengths, depending on η, and an electron may lose a considerable fraction of its energy through bremsstrahlung in passing through this material. The energy deposited in the calorimeter may be spread over a wide range in ϕ compared to the initial direction of the electron. To account for this in the reconstruction of electron candidates, clusters of calorimeter energy deposition ("superclusters") from a narrow fixed range in η and a variable range in ϕ are formed. Starting from these superclusters, corresponding hits in at least two layers of the pixel tracker capable of acting as seeds for electron trajectory candidates are required. Energy loss through bremsstrahlung leads to non-Gaussian contributions to fluctuations in the calorimeter and tracking measurements. Therefore, the seeding and building of tracks is done using dedicated algorithms designed to handle these fluctuations. The final fit of the trajectories relies on a Gaussian sum filter that is a non-linear generalization of the Kalman filter with weighted sums of Gaussians instead of a single Gaussian.

Muon candidates in CMS are identified from hits in the silicon tracking system and signals in the muon system [19, 20]. Since muons are typically the only particles reaching the muon chambers, the muon reconstruction algorithm begins with track segments detected in the innermost layers of these chambers. Additional hits in surrounding layers are then added. The tracks are propagated back to the interaction point, and a global fit is performed to match these tracks with consistent hits in the silicon tracker, producing a set of "global muon" candidates. A second reconstruction algorithm begins with tracks found in the tracking system and then associates them with compatible signals in the calorimeters and the muon chambers to produce "tracker muon" candidates. Muons in this analysis are required to be identified as both tracker muons and global muons.

Hadronic jets are reconstructed from individual particles whose identities and energies have been determined via a particle-flow technique [21] that combines information from all subdetectors: charged tracks in the tracker and energy deposits in the electromagnetic and hadronic calorimeters, as well as signals in the preshower detector and the muon system. The energy calibration is performed separately for

each particle type. All particles found by the particle-flow algorithm are clustered into particle-flow jets [22, 23] by using each particle's direction at the interaction vertex and the anti-k_T jet clustering algorithm [24] with the distance parameter $R = 0.5$, as implemented in FastJet version 2.4 [25].

Since most jet constituents are identified and reconstructed with nearly the correct energy by the particle-flow algorithm, only small residual jet energy corrections must be applied to each jet. These corrections are between 5% and 10% of the jet energy and were obtained as a function of p_T and η from the Geant4-based CMS Monte Carlo simulation (v. 9.2 Rev01) [26] and early collision data. The factors also include corrections for small discrepancies observed between the simulation and the data.

The missing transverse energy ($\not\!\!E_T$) is defined as the magnitude of the negative vector sum of the transverse energies (E_T) of all the particles found by the particle-flow algorithm. A decay of a $t\bar{t}$ pair via the lepton + jets channel is expected to exhibit significant missing transverse energy because of the undetected neutrino from the leptonically decaying W. Distributions of this variable are used in likelihood fits to measure the $t\bar{t}$ signal and to distinguish it from various backgrounds, as discussed in the following sections.

4 Data set and event selection

The data discussed in this paper were collected in the period April to November 2010 from proton-proton collisions at $\sqrt{s} = 7$ TeV and correspond to an integrated luminosity of 36 ± 1 pb^{-1} [27, 28]. The trigger providing the data sample used in this analysis is based on the presence of at least one charged lepton, either an electron or a muon. Because the peak instantaneous luminosity increased throughout the data-taking period, the minimum transverse momentum p_T of the muon required in the trigger ranged from 9 to 15 GeV, and the minimum E_T required in the trigger for electrons similarly ranged from 10 to 22 GeV. This data sample is used for the selection of the signal region and the selection of signal-depleted control regions used for studies related to background processes. Trigger efficiencies are determined from the data using Z-boson events and then corrected for the differences in the efficiencies between the Z-boson events and $t\bar{t}$ events, using the simulated samples described below. Events are required to have at least one primary pp interaction vertex, where vertices are identified by applying an adaptive fit to clusters of reconstructed tracks [29]. The primary vertex must be within ± 24 cm of the nominal interaction point in the direction along the proton beams. The distance between the primary vertex and the nominal interaction point in the plane perpendicular to the beam direction must be less than 2 cm.

In the event selection for the electron + jets channel, at least one electron with transverse energy greater than 30 GeV and $|\eta|$ less than 2.5 is required. Electrons from the transition region between the ECAL barrel and endcap, $1.44 < |\eta_{sc}| < 1.57$, are excluded, where η_{sc} is the pseudorapidity of the ECAL supercluster. The energy of the HCAL cell mapped to the supercluster must be less than 2.5% of the total calorimeter energy associated with the supercluster. Additional requirements are made on the shower shape and the angular separation between the ECAL supercluster and the matching track. Electron tracks must extrapolate to within 0.02 cm of the interaction vertex in the plane perpendicular to the proton beams and to within 1 cm in the direction along the beams. Electron candidates that lack hits in the inner layers of the tracking system are assumed to be the product of photon conversions and are discarded.

Since the electron from the W boson in a top-quark decay is expected to be isolated from other high-p_T particles in the event, electrons are required to have a relative isolation (I_{rel}) smaller than 0.1, where relative isolation is defined as the scalar sum of the transverse momenta of tracks with $p_T > 1$ GeV and all calorimeter energy in a cone of $\Delta R \equiv \sqrt{(\Delta\phi)^2 + (\Delta\eta)^2} < 0.3$ around the electron, divided by the electron p_T. Here $\Delta\phi$ ($\Delta\eta$) is the difference in azimuthal angle (pseudorapidity) between the electron and the track or calorimeter cell. Contributions to the sum due to the electron itself are removed. Events containing multiple electron candidates are rejected if any combined dielectron invariant mass lies within 15 GeV of the Z-boson mass.

In the event selection for the muon + jets channel, muons are required to have at least a minimum number of hits in both the silicon tracking system and the muon chambers. The muon must have transverse momentum greater than 20 GeV and must lie within the muon trigger acceptance ($|\eta| < 2.1$). Muons must extrapolate to within 0.02 cm of the interaction vertex in the plane perpendicular to the beams and to within 1 cm in the direction along the beams. The muon from the W boson in a top decay is also expected to be isolated from other high-p_T particles in the event, and thus muons are required to have relative isolation smaller than 0.05, where the muon relative isolation is defined analogously to the electron I_{rel}. These isolated muons must be separated from any selected jet (defined below) in the event by $\Delta R > 0.3$. Exactly one muon passing all these criteria is required. Events containing a separate, more loosely-defined muon, as well as the highly-energetic isolated muon described above, are rejected.

Z-boson events are used to study lepton trigger, identification, and isolation efficiencies in the data. A high purity Z-boson sample is extracted from data by requiring two oppositely-charged like-flavor leptons with a combined invariant mass within 15 GeV of the Z-boson mass. The two-electron final state suffers from background contamination due to hadronic jets misidentified as electrons. This

contamination is modeled using events containing a pair of like-charged electrons whose invariant mass falls within the Z-boson mass window. The identification efficiency for isolated electrons is determined to be 0.75, with combined statistical and systematic uncertainty (stat. + syst.) of ± 0.01. The trigger efficiency for such electrons is measured to be 0.982 ± 0.001 (stat.). Using $Z \to \mu\mu$ events, the efficiency of finding an isolated muon is measured to be 0.880 ± 0.002 (stat. + syst.), and the efficiency for triggering on muons passing all selection cuts is found to be 0.922 ± 0.002 (stat.).

Selected jets are required to have a jet-energy-scale-corrected $p_{\mathrm{T}} > 30$ GeV, $|\eta| < 2.4$, and must be separated by $\Delta R > 0.3$ from any isolated electrons and $\Delta R > 0.1$ from any isolated muons in order to remove jet candidates produced by charged leptons. Both the muon + jets and electron + jets analyses require that events contain at least three jets. Selected events are grouped into subsamples based on their jet multiplicity, so that events containing exactly three jets are separated from those containing four or more jets. A requirement on $\not\!\!E_{\mathrm{T}}$ is not included in the event selection, as fits to the distribution of this observable are used to separate the $\mathrm{t\bar{t}}$ signal from the backgrounds.

Dilepton $\mathrm{t\bar{t}}$ decays are removed by discarding events that contain both a high-p_{T} electron and a high-p_{T} muon. In the electron + jets event selection, events containing any muon with $p_{\mathrm{T}} > 10$ GeV, $|\eta| < 2.5$, and relative isolation < 0.2 are rejected. In the muon + jets event selection, events must contain no electron candidates with $E_{\mathrm{T}} > 15$ GeV and $I_{\mathrm{rel}} < 0.2$.

5 Simulation of signal and background events

We determine the efficiency for selecting lepton + jets signal events by using a simulated $\mathrm{t\bar{t}}$ event sample. We perform the simulation of signal $\mathrm{t\bar{t}}$ events using MadGraph (v. 4.4.12) [30], where the top-antitop pairs are generated accompanied by up to three additional hard jets in the matrix-element calculation. The factorization and renormalization scales Q^2 for $\mathrm{t\bar{t}}$ are both set to

$$Q^2 = m_{\mathrm{top}}^2 + \sum p_{\mathrm{T}}^2, \tag{1}$$

where m_{top} is the top-quark mass and $\sum p_{\mathrm{T}}^2$ is the sum of the squared transverse momenta of all accompanying hard jets in the event. MadGraph is also used to generate background events from electroweak production of single top quarks, the production of leptonically-decaying W and Z bosons in association with up to four extra jets, and photon + jets processes. The factorization and renormalization scales in these events are set in the same manner as for $\mathrm{t\bar{t}}$ events, with the appropriate boson mass replacing the top-quark mass. The parton-level results generated by MadGraph are next processed with Pythia (v. 6.420) [31] to provide showering of the generated particles. Shower matching is done by applying the MLM prescription [32]. Events are then passed through the Geant4-based CMS detector simulation.

In addition to the simulated events generated with MadGraph, several QCD multijet samples have been produced using Pythia. Samples enriched in electrons (muons) are used to provide a preliminary estimate on the QCD background in the electron + jets (muon + jets) channel. The final QCD background contribution is taken directly from data, as is explained in Sect. 6.

The $\mathrm{t\bar{t}}$ NLO production cross section has been calculated as $\sigma_{\mathrm{t\bar{t}}} = 157^{+23}_{-24}$ pb, using MCFM [33, 34]. For both $\mathrm{t\bar{t}}$ and single-top-quark production (described below), renormalization and factorization scales were set to $Q^2 = (172.5\ \mathrm{GeV})^2$. The uncertainty in the cross section due to uncertainties in these scales is determined by varying the scales by factors of 4 and 0.25 around their nominal values. Contributions to the cross section uncertainty from the parton distribution functions (PDF) and the value of α_S are determined following the procedures from the MSTW2008 [35], CTEQ6.6 [36], and NNPDF2.0 [37] sets. The uncertainties are then combined according to the PDF4LHC prescriptions [38].

The t-channel single-top-quark NLO cross section (multiplied by the leptonic branching fraction of the W boson) has been determined as $\sigma_{\mathrm{t}} = 21.0^{+1.1}_{-1.0}$ pb using MCFM [33, 39–41], where the uncertainty is defined similarly as for $\mathrm{t\bar{t}}$ production. The inclusive single-top-quark associated production (tW) NLO cross section of $\sigma_{\mathrm{tW}} = 10.6 \pm 0.8$ pb [40] has been used. Both cross sections include the production of single top and single antitop quarks. The inclusive s-channel single-top production cross section has been calculated using MCFM as 4.2 ± 0.2 pb. Because this cross section is small compared to the t-channel and tW production cross sections, it is treated as negligible in this analysis.

The NNLO production cross section for W bosons decaying into leptons has been determined to be $\sigma_{\mathrm{W}\to\ell\nu} = 31.3 \pm 1.6$ nb using FEWZ [42]. Its uncertainty was determined in a similar manner as for top-quark pair production. Finally, the Drell-Yan dilepton ($\ell\ell$) production cross section at NNLO has been calculated using FEWZ as $\sigma_{\mathrm{Z}/\gamma^*\to\ell\ell}(\mathrm{m}_{\ell\ell} > 20\ \mathrm{GeV}) = 5.00 \pm 0.27$ nb and $\sigma_{\mathrm{Z}/\gamma^*\to\ell\ell}(\mathrm{m}_{\ell\ell} > 50\ \mathrm{GeV}) = 3.05 \pm 0.13$ nb. Backgrounds due to diboson production have been ignored given their relatively small expected contribution to the lepton + jets event yield.

In a simulated sample of $\mathrm{t\bar{t}}$ events in which all top-quark decay modes are included, the electron + jets selection efficiency is found to be 5.7%, while the muon + jets selection efficiency is 7.2%. The selected simulated signal events in each mode are dominated by $\mathrm{t\bar{t}}$ decays to electron + jets

Table 1 Predicted event yields for the electron + jets and muon + jets event selections. The event yields from the simulation are normalized to an integrated luminosity of 36 pb^{-1}. The quoted uncertainties account for the limited number of simulated events, the uncertainty on the calculated cross section (where available), the uncertainties on the lepton selection and trigger efficiency correction factors, and a 4% uncertainty on the luminosity. The penultimate row lists the totals from the simulation, and the last row shows the number of observed events

	Electron + jets		Muon + jets	
	$N_{\text{jets}} = 3$	$N_{\text{jets}} \geq 4$	$N_{\text{jet}} = 3$	$N_{\text{jets}} \geq 4$
$t\bar{t}$	157 ± 25	168 ± 27	197 ± 31	211 ± 33
Single top	22 ± 1	9 ± 1	30 ± 1	11 ± 1
W + jets	374 ± 27	94 ± 7	486 ± 34	115 ± 9
Z + jets	66 ± 5	15 ± 1	46 ± 3	11 ± 1
QCD	314 ± 19	53 ± 8	49 ± 3	9 ± 1
Sum (simulated events)	934 ± 55	339 ± 32	807 ± 53	358 ± 37
Observed in data	1183	428	1064	423

and muon + jets, respectively, although $t\bar{t}$ decays containing tau leptons also contribute. Table 1 and Fig. 1 give the observed numbers of events in both channels after applying the event selection procedures described above to the pp collision data set. The numbers of events predicted by the simulation for the different physics processes are also listed. Predicted yields are calculated by multiplying selection efficiencies for each process, as determined from simulation, by the appropriate NLO or NNLO cross sections and the total integrated luminosity of 36 pb^{-1}. As shown in Fig. 1, the fractional contribution to the event yield from $t\bar{t}$ signal events is negligible in events with zero jets, but dominates as jet multiplicity increases. More events are observed in the data than predicted by the simulation, indicating that either the signal cross section or the background cross sections, or possibly both, are larger than expected. Our method for determining the number of signal and background events in the data is described in the next section.

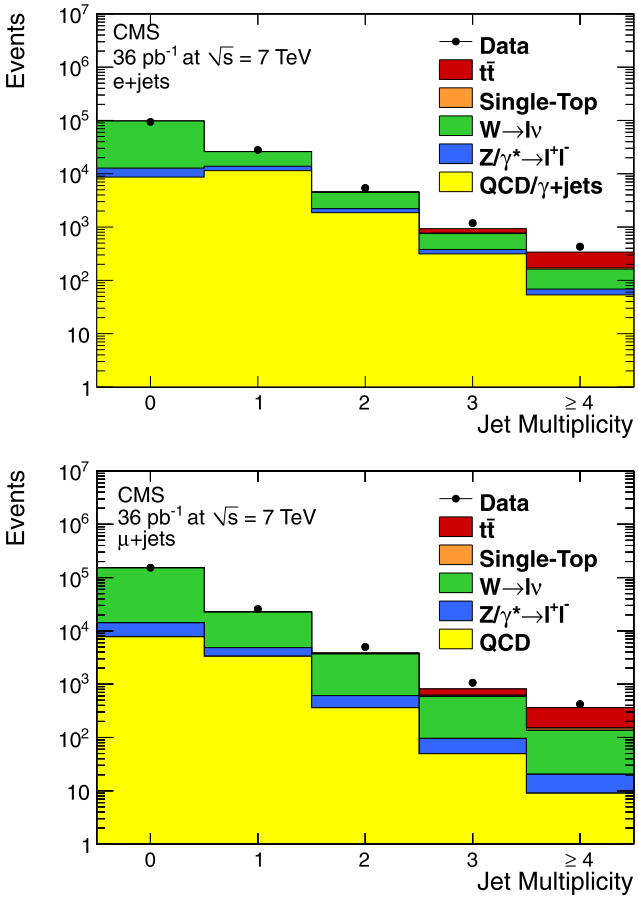

Fig. 1 Observed numbers of events from data and simulation as a function of jet multiplicity in the (*top*) electron + jets and (*bottom*) muon + jets selected samples. Yields are calculated after applying the respective event selections and omitting any requirement on the number of jets

6 Cross-section measurement

6.1 Analysis method

We measure the $t\bar{t}$ cross section in a data sample consisting of events with leptons and jets in the final state. Since the event yields for the background processes can be difficult to estimate purely from simulations, the kinematic properties of the events are used to separate signal from background. It would be natural to require four or more jets for the selection of $t\bar{t}$ events in the lepton + jets channel, owing to the four final-state quarks present in these decays and because the number of background events from W/Z + jets and QCD multijet events decreases with increasing jet multiplicity. However, it is also useful to include events with only three jets in the selection. In addition to improving the overall signal efficiency, the inclusion of three-jet events constrains the QCD and W + jet background normalization when a simultaneous fit to the three-jet and inclusive four-jet samples is performed.

The predicted jet-multiplicity distribution and the predicted ratio between events with three jets and events with four or more jets for the different processes are used to simultaneously fit the fraction of $t\bar{t}$ events and the contamination from background processes. Kinematic variables whose shapes are different for the different processes are used to separate the backgrounds from the signal. After a number of variables and combinations were tested, the variable M3 was chosen to separate $t\bar{t}$ events from background events in the inclusive four-jet sample. This variable is defined as the invariant mass of the combination of the three jets with the largest vectorially summed transverse momentum. It approximates the mass of the hadronically-decaying top quark and thus provides good separation power. The three-jet sam-

ple is dominated by W + jets events and QCD multijet events. For the three-jet sample, a variable that is well suited for the discrimination of QCD multijet events from the other processes is needed. In contrast to processes with W bosons, QCD processes exhibit only small amounts of missing transverse energy, mostly because of mismeasured jets rather than the presence of neutrinos. Therefore $\not\!\!E_{\mathrm{T}}$ was chosen as the discriminating variable to separate QCD events from W + jets and $\mathrm{t\bar{t}}$ signal events in the three-jet sample.

The $\not\!\!E_{\mathrm{T}}$ and M3 distributions from the observed data sample are fit simultaneously to obtain the contributions of the signal and the main background processes. We use a binned likelihood fit, where the number of expected events $\mu_j[i]$ in each bin i of the distribution for the variable of choice j (either $\not\!\!E_{\mathrm{T}}$ or M3) is compared to the observed number of events in this bin. The number of expected events in bin i is given by:

$$\mu_j[i] = \sum_k \beta_k \cdot \alpha_{jk}[i], \tag{2}$$

where α_{jk} is the binned contribution (called "template" in the following) for variable j and process k. The fit parameters β_k are the ratio of the measured (σ_k) and predicted (σ_k^{pred}) cross sections for process k:

$$\beta_k = \frac{\sigma_k}{\sigma_k^{\mathrm{pred}}}. \tag{3}$$

Here, k denotes all processes that are taken into account, namely $\mathrm{t\bar{t}}$, W + jets, Z + jets, single-top-quark decays, and QCD. Since negative β_k values are unphysical, we do not allow β_k to become smaller than zero in the fit. The templates α_{jk} are normalized to the corresponding predictions for process k for events with three jets and events with four or more jets. Because of the normalization of the fit templates to the prediction, the fitted value of β_k can be directly interpreted as the scale factor one has to apply to the predicted cross section of a given process k to derive the measured cross section.

Templates for the $\mathrm{t\bar{t}}$, single-top, W + jets, and Z + jets processes are derived from the simulation, while the QCD multijet template is derived from data, using a method that will be described later. The shapes of the M3 and $\not\!\!E_{\mathrm{T}}$ distributions of single-top-quark events are very similar to the distributions of $\mathrm{t\bar{t}}$ events. Because of this similarity and because of the very small number of expected single-top-quark events, an unconstrained fit of the single-top-quark contribution is not possible. However, since the single-top-quark production process is theoretically well understood, the number of such events can be estimated from simulations. Therefore the fit parameter for single top is not left to float freely, but is instead subject to a Gaussian constraint with a mean of 1.0 and width of 0.3. The uncertainty on this value is assigned according to the expected precision of initial single-top cross-section measurements in CMS [43]. In addition, the ratio between the W + jets and Z + jets cross sections is constrained to be within 30% of the expectation from theory, where the constraint width is set by the uncertainty in the NLO cross sections [44]. These constraints are inserted by multiplying the likelihood function used in the fit by Gaussian terms of mean value 1.0 and widths corresponding to the uncertainties on the respective constraints. The same β_k parameters are used for both jet-multiplicity bins.

A Neyman construction [45] with central intervals and a maximum-likelihood estimate of the $\mathrm{t\bar{t}}$ cross section as test statistic was chosen to obtain the confidence interval for the $\mathrm{t\bar{t}}$ cross section. For this purpose pseudo-experiments are performed in which the number of events from the different processes are chosen randomly around the values predicted by simulations within appropriate uncertainties. Specifically this is done by randomly choosing, for each background process, an input value for β_k from a normal distribution with mean value 1.0 and a width of 30% for W + jets, Z + jets, and single top. Since the properties of QCD multijet events are more difficult to calculate, a more conservative uncertainty of 50% is used for this background. The templates for the different processes are then scaled with the corresponding β_k values and summed together, generating a pseudo-data distribution for $\not\!\!E_{\mathrm{T}}$ in the three-jet sample and a pseudo-data distribution for M3 in the inclusive four-jet sample. To simulate statistical fluctuations we then vary the contents of each bin of the two distributions using Poisson statistics. A maximum-likelihood fit to the templates is then performed on the distributions. This procedure yields one signal fit result $\beta_{\mathrm{t\bar{t}}}^{\mathrm{fit}}$ for each pseudo-experiment and provides a measurement of any possible bias between the input and fitted values. We vary the input value $\beta_{\mathrm{t\bar{t}}}^{\mathrm{in}}$ between 0.0 and 3.0 in steps of 0.2, and perform 50 000 pseudo-experiments for each value. Each set of pseudo-experiments gives a distribution of the fitted values $\beta_{\mathrm{t\bar{t}}}^{\mathrm{fit}}$. For each input value we determine the median and the 68% and 95% quantiles of the corresponding $\beta_{\mathrm{t\bar{t}}}^{\mathrm{fit}}$ distribution and use these values for the estimation of the central values and for the construction of confidence belts, respectively. From this confidence-belt construction the $\mathrm{t\bar{t}}$ cross section result corresponding to the $\beta_{\mathrm{t\bar{t}}}^{\mathrm{fit}}$ measured in data can be extracted together with its total uncertainty. By construction, this treatment the correct coverage probability.

6.2 Systematic uncertainties

In general, the presence of a systematic uncertainty affects both the number of selected events and the shape of the investigated discriminating observables, resulting in modified

distributions $\alpha_{jk}^{\text{syst}}$ for the different processes. In order to estimate the effect of different sources of systematic uncertainties we construct modified templates and draw the pseudo-data used for the statistical calculation from them. For each source of systematic uncertainty u, two templates $\alpha_{jk}^{u,+1}$ and $\alpha_{jk}^{u,-1}$, corresponding to variations of ± 1 standard deviation ($\pm 1\sigma$) of the specific systematic uncertainty, are used. Both templates are normalized to the altered event yields for each specific systematic uncertainty u, and thus account for both changes in event rates and changes in parameter distributions. These $\pm 1\sigma$ templates are derived either by altering the nominal samples as described in the following sections or from dedicated simulations. The modified α_{jk}^{u} used for drawing the pseudo-data can then be constructed from the nominal template α_{jk} and the $\alpha_{jk}^{u,\pm 1}$ templates. Therefore for each uncertainty u a strength parameter δ_u is introduced, and $\alpha_{jk}^{\text{syst}}$ is defined as a linear interpolation:

$$\alpha_{jk}^{\text{syst}}[i] = \alpha_{jk}[i] + \sum_{u} |\delta_u| \cdot \left(\alpha_{jk}^{u,\text{sign}(\delta_u)}[i] - \alpha_{jk}[i]\right). \quad (4)$$

Here, u runs over all sources of systematic uncertainties and $\alpha_{jk}^{u,\pm 1}[i]$ is the prediction for bin i of distribution j of process k affected by $+1\sigma$ or -1σ of uncertainty u. Random numbers following a Gaussian distribution with a mean of zero and unit width are used as values for each δ_u, with the strengths determined separately for each pseudo-experiment. The nominal template is reproduced for $\delta_u = 0$, while the two altered templates correspond to $\delta_u = +1$ and $\delta_u = -1$. For all other values of δ_u, the desired mixture of the nominal and shifted templates is obtained.

In order to prevent unphysical negative predictions for a process, the linear interpolation is cut off at a bin content of zero, i.e., whenever a bin of $\alpha_{jk}^{\text{syst}}$ calculated according to (4) has a value less than zero, zero is used instead. The definition of $\beta_{\text{t}\bar{\text{t}}}^{\text{fit}}$ remains unchanged, meaning that the original templates without uncertainties are employed for fitting the pseudo-data distributions.

The influence on our measurement due to the imperfect knowledge of the jet energy scale (JES) is estimated by simultaneously varying all jet four-momenta either by $+1\sigma$ or by -1σ of the energy scale uncertainties, which are functions of the jet η and p_{T}. These uncertainties on the particle-flow jet energy scale are typically about 3%, as shown in Ref. [46]. In addition, a constant 1.5% uncertainty due to changes in calorimeter calibrations and a p_{T}-dependent uncertainty of 1.32 GeV$/p_{\text{T}}$ due to multiple collisions in the same event ("pileup") are applied. For jets that can be matched to a b quark at the parton level, we assign an additional uncertainty of 2% if the jet lies within $|\eta| < 2.0$ and has p_{T} between 50 GeV and 200 GeV, and a 3% uncertainty otherwise. This uncertainty accounts for observed response differences for b jets generated in PYTHIA and those in HERWIG [47]. The overall uncertainty is determined by adding all of the individual uncertainties in quadrature.

Jet asymmetry measurements suggest that the jet energy resolutions (JER) in data are about 10% worse than in the simulation [48]. The uncertainty on this measurement is also about 10%. To account for this, jets in the simulated samples are altered so that their resolutions match those measured in data, and the effect is propagated to the calculation of $\not\!\!E_{\text{T}}$. The impact of this uncertainty on our measurement is determined by evaluating the change in cross section when simulated jet resolutions are widened by 0% or 20%, rather than the default 10%.

The corrections in jet energy scale and resolution described above are used to vary the missing transverse energy according to variations in clustered jet energy. In order to also account for the uncertainty of unclustered energy in $\not\!\!E_{\text{T}}$, the amount of unclustered energy contributing to $\not\!\!E_{\text{T}}$ is shifted by $\pm 10\%$. However, the impact of the variation of the unclustered energy on the measurement is found to be negligible.

Adjusted simulated samples are used to evaluate the dominant systematic uncertainites in the cross section measurements. Two simulated samples of $\text{t}\bar{\text{t}}$ events are available to estimate the systematic uncertainty induced by the lack of accurate knowledge of the amount of QCD initial-state (ISR) and final-state (FSR) radiation. For one of these samples, the amount of ISR and FSR has been increased, while less ISR and FSR is assumed in the other sample.

The impact of uncertainties in the factorization scales on the cross section measurement is estimated by varying the scales in each of the samples by factors of 0.25 and 4.0 with respect to their default values. The W + jets and Z + jets processes are treated as being correlated, and their respective factorization scales are shifted either down or up simultaneously, while the $\text{t}\bar{\text{t}}$ scale is considered to be uncorrelated and is shifted independently. The impact of a variation of the shower matching threshold is investigated by varying the matching thresholds for the three processes by factors of 0.5 and 2.0 compared to the default thresholds. Again, W + jets and Z + jets processes are treated as fully correlated and are varied simultaneously, while the $\text{t}\bar{\text{t}}$ process is considered uncorrelated and therefore independently altered.

The measurement of the electron E_{T} has a relative uncertainty of 2.5% in the endcap region, while the uncertainties for the barrel region and for muons can be neglected. These variations in the electron energy scale are also propagated to the missing transverse energy. This component of the $\not\!\!E_{\text{T}}$ uncertainty is treated as uncorrelated with the other $\not\!\!E_{\text{T}}$ uncertainties.

Correction factors have been applied to match the trigger-selection and lepton-selection efficiencies in simulated samples with those in data. These factors are obtained from data by using decays of Z bosons to dileptons. In the electron +

jets channel, the correction factor is 0.933 ± 0.032. In the muon + jets channel, it is 0.965 ± 0.004. The uncertainty on the $\mathrm{t\bar{t}}$ cross section measurement due to the uncertainties of the correction factors is evaluated by weighting all simulation-based samples according to the $\pm 1\sigma$ uncertainties obtained from these studies.

We evaluated the systematic uncertainty on the $\mathrm{t\bar{t}}$ cross section measurement induced by the imperfect knowledge of the PDF of the colliding protons using the CTEQ6.6 [49] PDF set and the LHAPDF [50] package. For this purpose, a reweighting procedure is applied to all generated samples, in which each CTEQ6.6 PDF parameter is independently varied by its positive and negative uncertainties, with a new weight assigned to each variation. The resulting templates are used to estimate the impact of variations in the PDFs on our measurement.

The default samples used for this analysis were produced without any pileup collisions. These samples are insufficient for the simulation of data taken in late 2010, when the instantaneous luminosity was substantially higher than in early data-taking and roughly four to five additional collisions per bunch crossing were expected. In order to estimate the effect of these pileup collisions, which are present in data but not in our fit templates, additional samples of $\mathrm{t\bar{t}}$ and W + jets events that included the simulation of these extra collisions were produced. Although the average number of pileup collisions in these samples is slightly larger than the expected number in data, these simulated events can still be used to provide a conservative estimation of the impact of pileup collisions on our measurement.

6.3 Electron + jets analysis

In the electron + jets channel, we model $\mathrm{t\bar{t}}$, W + jets, Z + jets, and single-top-quark production using the simulated event samples described previously. For the QCD multijet background, a sideband method based on data is used to model the M3 and $\not\!\!E_{\mathrm{T}}$ distributions, where the sidebands are chosen to be depleted in contributions from real W bosons. In the sideband selection, events must have an electron that fails at least two of the three quality requirements: $I_{\mathrm{rel}} < 0.1$ (but $I_{\mathrm{rel}} < 0.5$ is always required), transverse impact parameter < 0.02 cm, and the standard electron identification criteria. As verified with simulated events, the data sample extracted in this way has a QCD multijet purity larger than 99%. In addition, the M3 and $\not\!\!E_{\mathrm{T}}$ shapes derived from this sample are in good agreement with the distributions from the simulation. The fraction of events in the three-jet and inclusive four-jet sample for each process are taken from the simulation. Figure 2 shows the distributions of $\not\!\!E_{\mathrm{T}}$ and M3 from the simulated three-jet and inclusive four-jet samples, respectively, for the different processes.

The modeling of QCD multijet events from data might induce an additional source of systematic uncertainty. This is investigated by separating the sideband region from which the QCD templates are derived into two parts. The sideband region is defined, in addition to other criteria, by $0.1 < I_{\mathrm{rel}} < 0.5$ for the electron + jets channel. The QCD template is further split into two separate samples of equal-width regions in I_{rel} ($0.1 < I_{\mathrm{rel}} < 0.3$ and $0.3 < I_{\mathrm{rel}} < 0.5$), and the templates from these two samples are used to estimate this systematic uncertainty. The uncertainty in the ratio of the number of events with three jets to that with four or more jets is investigated as well. While this ratio for the model predictions is taken from the simulation, the observed ratio in the sideband selection is different. Consequently, the two potential sources of systematic uncertainties are studied separately via two independent strength parameters.

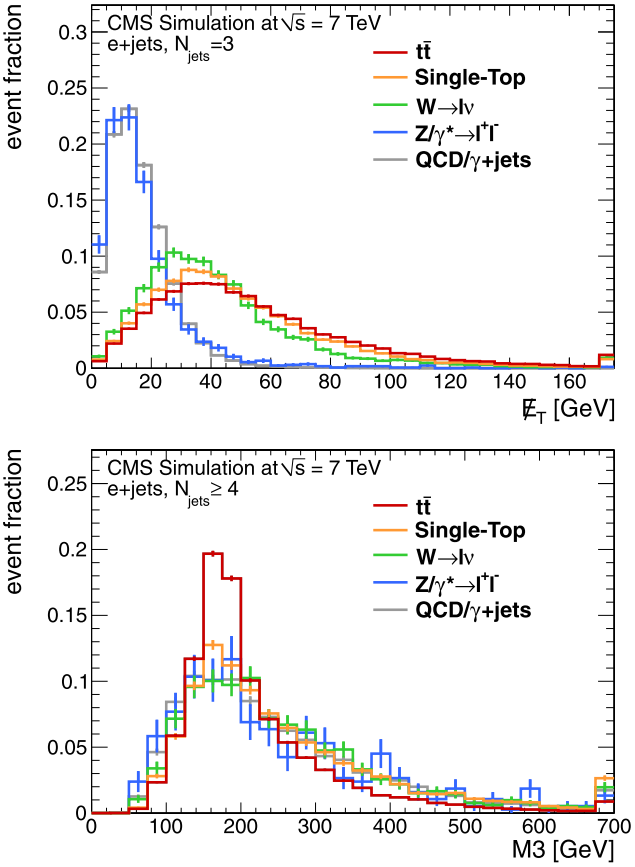

Fig. 2 (Color online) Simulated distributions from electron + jets events of (*top*) $\not\!\!E_{\mathrm{T}}$ for events with three jets and (*bottom*) M3 for events with four or more jets. The contributions from the different processes are shown separately, and are normalized to unity. Error bars are statistical only

The $\mathrm{t\bar{t}}$ cross section is measured, accounting for statistical and systematic uncertainties, using the fit method described in Sect. 6.1. The parameter $\beta_{\mathrm{t\bar{t}}}^{\mathrm{fit}}$, which is used to compute the $\mathrm{t\bar{t}}$ cross section, and the values of β_k for the background processes are determined in the fit. The results for $\beta_{\mathrm{t\bar{t}}}$ and the signal and background event yields for the inclusive three-jet bin are given in Table 2. While the number of fitted $\mathrm{t\bar{t}}$ events

Table 2 The predicted and fitted values for $\beta_{\mathrm{t\bar{t}}}$ and for the numbers of events for the various contributions from the inclusive three-jet electron + jets sample. The quoted uncertainties in the $\mathrm{t\bar{t}}$ yield account for statistical and systematic uncertainties, while the uncertainties in the background event yields are derived from the covariance matrix of the maximum-likelihood fit and therefore represent purely statistical uncertainties

	$\beta_{\mathrm{t\bar{t}}}$	$N_{\mathrm{t\bar{t}}}$	$N_{\text{single-top}}$	$N_{\text{W+jets}}$	$N_{\text{Z+jets}}$	N_{QCD}
Electron + jets (predicted)	1.00	325 ± 52	31 ± 2	468 ± 34	81 ± 6	367 ± 27
Electron + jets (fitted)	$1.14^{+0.29}_{-0.24}$	371^{+94}_{-78}	33 ± 9	669 ± 61	116 ± 36	422 ± 51

$N_{\mathrm{t\bar{t}}}$ is quoted with its combined statistical and systematic uncertainty, for the remaining processes only statistical uncertainties are given. A list of all systematic uncertainties in this channel is provided in Sect. 6.5, with the dominant systematic uncertainty coming from the lack of knowledge of the jet energy scale.

In the electron + jets channel, the resulting $\mathrm{t\bar{t}}$ production cross section is:

$$\sigma_{\mathrm{t\bar{t}}} = 180^{+45}_{-38}\,(\text{stat.} + \text{syst.}) \pm 7\,(\text{lumi.})\ \text{pb}. \tag{5}$$

The fit produces a combined statistical and systematic uncertainty, as given above. A fit using only the nominal templates yields a statistical uncertainty of $^{+23}_{-22}$ pb. Assuming uncorrelated, Gaussian behavior of statistical and systematic uncertainties, one can subtract the statistical uncertainty in quadrature from the overall uncertainty, resulting in a systematic uncertainty of $^{+39}_{-31}$ pb. Individual uncertainties are summarized in Sect. 6.5.

The measured $\mathrm{t\bar{t}}$ cross section, in combination with the background estimation, can be used to compare distributions of $\not\!\!E_{\mathrm{T}}$ and M3 found in data with those predicted by Monte Carlo simulation. Figure 3 shows the distributions of the missing transverse energy and M3 as observed in data. For comparison, the templates from simulation are normalized to the fitted fractions. The deviation visible in the high-M3 region between simulation and data has been investigated using pseudo-experiments including statistical and systematic uncertainties. For 10% of the simultaneous fits to $\not\!\!E_{\mathrm{T}}$ and M3 in these pseudo-experiments, the derived Kolmogorov–Smirnov (KS) value is larger than the KS value observed in data. Therefore, the observed deviation in the M3 distribution is not outside the range of expected fluctuations.

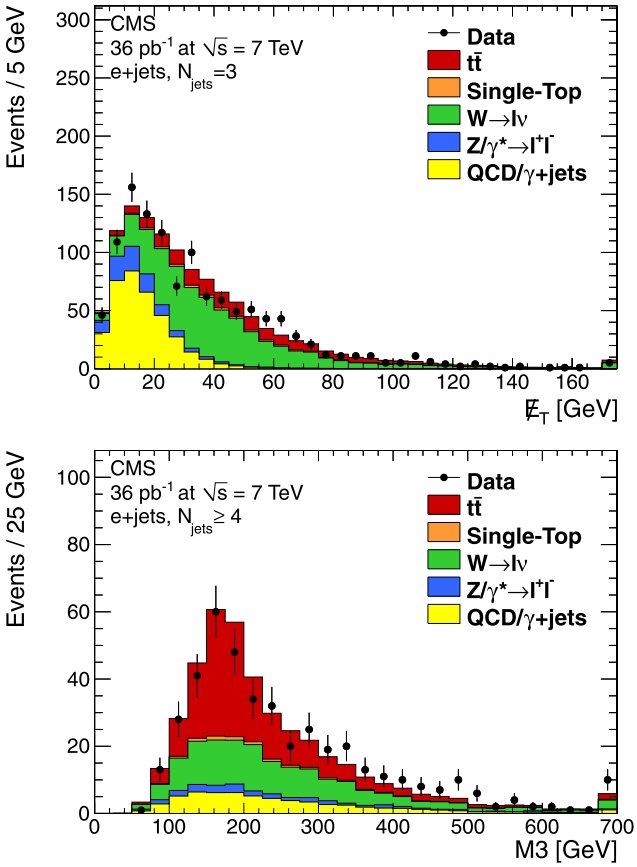

Fig. 3 Electron + jets channel: Comparison of the distributions in data and simulation of the discriminating variables $\not\!\!E_{\mathrm{T}}$ (*top*) and M3 (*bottom*) for signal and background. The simulation has been normalized to the fit results. Only statistical uncertainties are shown

6.4 Muon + jets analysis

The same analysis method is used to measure the $\mathrm{t\bar{t}}$ cross section in the muon + jets final state. $\not\!\!E_{\mathrm{T}}$ and M3 are again used as discriminating variables. Shape comparisons for the different physics processes are shown in Fig. 4. In the muon + jets channel, the QCD templates for these two distributions are derived from data by selecting events in a sideband region enriched in QCD multijet events. The relative isolation is required to be between 0.2 and 0.5 for the sideband selection, in contrast to the nominal selection, where the muon must have a relative isolation smaller than 0.05. The gap between the allowed isolation ranges in the two selections reduces the signal events contribution to the sideband. Events containing muons with large relative-isolation values have different kinematics due to the correlation of the relative isolation with transverse momentum. We therefore restrict I_{rel} to be smaller than 0.5. The QCD multijet purity as measured from simulation is 98.4% in the three-jet sample and 94.3% for events with four or more jets. As in the electron + jets channel, the QCD template is split into two

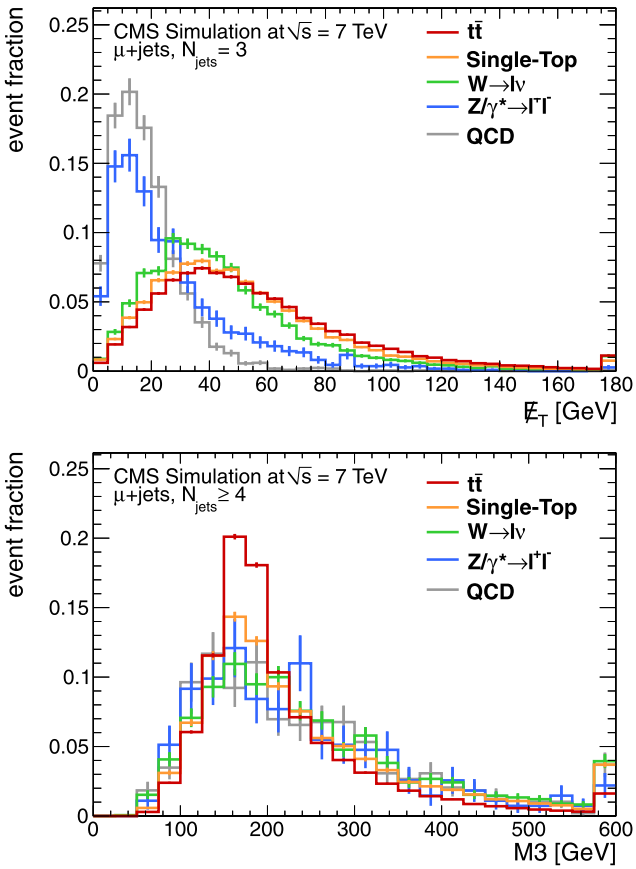

Fig. 4 (Color online) Simulated distributions from muon + jets events of (*top*) $\not\!\!E_T$ for events with three jets and (*bottom*) M3 for events with four or more jets for the different processes. The contributions from the different processes are shown separately, and are normalized to unity. Error bars are statistical only

separate samples of equal-width regions in I_{rel}, and the templates from these two samples are used to estimate the systematic uncertainty on the QCD modeling. Apart from the electron energy scale, all other systematic uncertainties described in the previous section are also accounted for in the muon + jets analysis. A summary of the individual contributions from the various sources of systematic uncertainties is provided in Sect. 6.5.

The results for $\beta_{\mathrm{t\bar{t}}}$ and the various background yields from the binned likelihood fit to the inclusive three-jet muon + jets sample are given in Table 3. Using the method described in Sect. 6.1, the fitted value $\beta_{\mathrm{t\bar{t}}}$ and the $\pm 1\sigma$ statistical + systematic uncertainties corresponding to the fitted value $\beta_{\mathrm{t\bar{t}}}^{\mathrm{fit}} = 1.07$ are determined. The result of the muon + jets analysis is a measured $\mathrm{t\bar{t}}$ production cross section of:

$$\sigma_{\mathrm{t\bar{t}}} = 168^{+42}_{-35}\,(\mathrm{stat.} + \mathrm{syst.}) \pm 7\,(\mathrm{lumi.})\ \mathrm{pb}. \quad (6)$$

The statistical uncertainty is $^{+18}_{-17}$ pb. With the assumption that the statistical and systematic uncertainties are Gaussian and uncorrelated, the systematic uncertainty is calculated to be $^{+38}_{-31}$ pb. Similar to the measurement in the electron + jets channel, the fitted numbers of W + jets, Z + jets events and QCD multijet events are found to exceed the predicted values. The KS p-value of this fit result has been determined to be 95%. Figure 5 shows comparisons of the distributions of $\not\!\!E_T$ and M3 between data and simulation, where the simulation has been scaled to the results obtained from the binned likelihood fit.

6.5 Combined electron+jets and muon + jets analysis

The $\mathrm{t\bar{t}}$ cross section is also determined using the method described in Sect. 6.1 for the combined electron + jets and muon + jets channel. Simultaneous fits of the $\not\!\!E_T$ and M3 distributions are performed in both the electron + jets and muon + jets channels. Six fit parameters are used: the fraction of $\mathrm{t\bar{t}}$ events ($\beta_{\mathrm{t\bar{t}}}$), the fractions of the different background processes (β_{t}, β_{W}, and β_{Z}), and two distinct fractions of QCD multijet events ($\beta_{\mathrm{QCD},e}$ and $\beta_{\mathrm{QCD},\mu}$). The use of two fit parameters for the fraction of QCD multijet events is motivated by the fact that the sources of such events contributing to this background in the electron + jets channel are very different from those contributing to the muon + jets channel. The cross section was determined with the same procedure used for the individual electron and muon channels. Figure 6 shows the Neyman construction with all systematic uncertainties included for the combined measurement. The fitted $\beta_{\mathrm{t\bar{t}}}$ parameter and the fitted numbers of events for the various background processes are summarized in Table 4.

The fitted $\beta_{\mathrm{t\bar{t}}}$ value corresponds to a measured $\mathrm{t\bar{t}}$ cross section in the lepton + jets channel of

$$\sigma_{\mathrm{t\bar{t}}} = 173^{+39}_{-32}\,(\mathrm{stat.} + \mathrm{syst.}) \pm 7\,(\mathrm{lumi.})\ \mathrm{pb}. \quad (7)$$

Table 3 The predicted and fitted values for $\beta_{\mathrm{t\bar{t}}}$ and for the numbers of events for the various contributions from the inclusive three-jet muon + jets sample. The quoted uncertainties in the $\mathrm{t\bar{t}}$ yield account for statistical and systematic uncertainties, while the uncertainties in the background event yields are derived from the covariance matrix of the maximum-likelihood fit and therefore represent purely statistical uncertainties

	$\beta_{\mathrm{t\bar{t}}}$	$N_{\mathrm{t\bar{t}}}$	$N_{\mathrm{single\text{-}top}}$	$N_{\mathrm{W+jets}}$	$N_{\mathrm{Z+jets}}$	N_{QCD}
Muon + jets (predicted)	1.00	408 ± 64	41 ± 2	601 ± 43	57 ± 4	58 ± 4
Muon + jets (fitted)	$1.07^{+0.26}_{-0.24}$	437^{+106}_{-90}	41 ± 12	813 ± 59	76 ± 22	123 ± 33

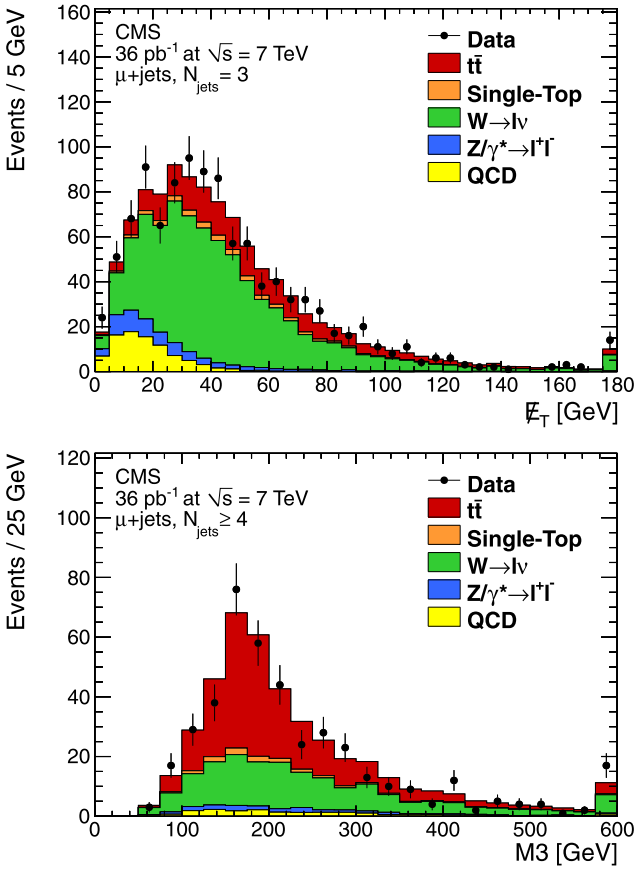

Fig. 5 Muon + jets channel: Comparison of the data distributions of the discriminating variables $\not\!\!E_T$ (*top*) and M3 (*bottom*) and the simulation of the different processes. The simulation has been normalized to the fit results

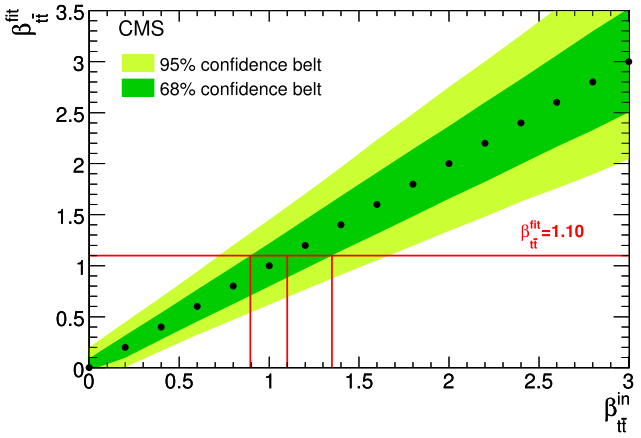

Fig. 6 Neyman construction including all systematic uncertainties for the combined measurement of the $t\bar{t}$ production cross section in the electron + jets and muon + jets channels. The *horizontal line* indicates the determined value $\beta_{t\bar{t}} = 1.10$ from the binned likelihood fit to observed pp collision data

The statistical uncertainty is 14 pb. Subtracting this in quadrature from the overall uncertainty yields a systematic uncertainty of $^{+36}_{-29}$ pb. The fit in the combined channel yields a KS p-value of 68% and agrees well with a simple average of the results in the muon and electron channels, while correctly accounting for correlations.

Table 5 gives an overview of the estimated statistical and systematic uncertainties for this combined measurement as well as for the two channels separately. The different sources of systematic uncertainties are treated as fully correlated between the two channels, except for flavor-specific QCD and lepton uncertainties, which are assumed to be uncorrelated.

In order to estimate the impact of individual systematic uncertainties, Neyman constructions where only the specific source of systematic uncertainty under study is accounted for are used. Each result indicates the combined statistical and systematic uncertainties of the contribution under study.

Combining both channels significantly reduces the statistical uncertainty in the measured cross section. However, since both single measurements are already dominated by systematic uncertainties, the improvement in the total uncertainty of the combined measurement is relatively small. One can see that the largest contributor to the overall systematic uncertainty is the uncertainty in the jet energy scale. Shifts in this scale lead to substantial changes in the jet selection efficiency for both signal and background processes, resulting in a large systematic uncertainty.

The transverse mass of the charged lepton and the $\not\!\!E_T$ is a kinematic variable that lacks the discriminating power of the M3 and $\not\!\!E_T$ variables for identifying $t\bar{t}$ decays. However, this variable does provide separation between events containing a decaying W boson and non-W-boson decays, and thus serves as an independent check of the kinematics of the simulated samples used in this analysis. Distributions of the transverse mass in the muon + jets and electron + jets channels are shown in Fig. 7 for events with three or more

Table 4 Predicted and fitted values for $\beta_{t\bar{t}}$ and for the numbers of events for the various contributions in the inclusive three-jet combined electron + jets and muon + jets sample. The quoted uncertainties in the $t\bar{t}$ yield account for statistical and systematic uncertainties, while the uncertainties in the background event yields are derived from the covariance matrix of the maximum-likelihood fit and therefore represent purely statistical uncertainties

	$\beta_{t\bar{t}}$	$N_{t\bar{t}}$	$N_{\text{single-top}}$	$N_{\text{W+jets}}$	$N_{\text{Z+jets}}$	N_{QCD} e + jets	N_{QCD} μ + jets
Predicted	1.00	733 ± 116	72 ± 4	1069 ± 77	138 ± 10	367 ± 27	58 ± 4
Fitted	$1.10^{+0.25}_{-0.21}$	806^{+183}_{-154}	76 ± 22	1475 ± 86	184 ± 51	440 ± 44	113 ± 31

Table 5 Relative statistical and systematic uncertainties in the estimation of the $t\bar{t}$ production cross section in the electron + jets and muon + jets channels, and their combination, assuming $\beta_{t\bar{t}} = 1$. The total ("stat. + syst.") uncertainty is obtained from a Neyman construction, for which all sources of systematic uncertainties are taken into account in the prior predictive ensembles. The estimate of each systematic uncertainty ("syst. only") is calculated by assuming uncorrelated, Gaussian behavior of the statistical and systematic uncertainties and subtracting the statistical uncertainty in quadrature from the total uncertainty

	Electron + jets channel		Muon + jets channel		Combined result	
	Stat. + syst. uncertainty	Syst. only	Stat. + syst. uncertainty	Syst. only	Stat. + syst. uncertainty	Syst. only
Stat. uncertainty	$^{+14.0\%}_{-13.1\%}$	–	$^{+11.4\%}_{-10.8\%}$	–	$^{+8.7\%}_{-8.4\%}$	–
JES	$^{+23.5\%}_{-20.4\%}$	$^{+18.9\%}_{-15.6\%}$	$^{+21.9\%}_{-18.8\%}$	$^{+18.7\%}_{-15.4\%}$	$^{+20.3\%}_{-17.6\%}$	$^{+18.3\%}_{-15.5\%}$
Factorization scale	$^{+15.5\%}_{-14.3\%}$	$^{+6.7\%}_{-5.7\%}$	$^{+13.8\%}_{-12.9\%}$	$^{+7.8\%}_{-7.1\%}$	$^{+11.2\%}_{-10.6\%}$	$^{+7.1\%}_{-6.5\%}$
Matching threshold	$^{+15.0\%}_{-14.0\%}$	$^{+5.4\%}_{-4.9\%}$	$^{+14.1\%}_{-12.9\%}$	$^{+8.3\%}_{-7.1\%}$	$^{+10.5\%}_{-9.8\%}$	$^{+5.9\%}_{-5.0\%}$
Pileup	$^{+14.4\%}_{-13.8\%}$	$^{+3.4\%}_{-4.3\%}$	$^{+11.7\%}_{-11.3\%}$	$^{+2.6\%}_{-3.3\%}$	$^{+9.3\%}_{-9.3\%}$	$^{+3.3\%}_{-4.0\%}$
ID/reconstruction	$^{+14.5\%}_{-13.6\%}$	$^{+3.8\%}_{-3.7\%}$	$^{+11.9\%}_{-11.2\%}$	$^{+3.4\%}_{-3.0\%}$	$^{+9.2\%}_{-8.7\%}$	$^{+3.0\%}_{-2.3\%}$
QCD rate & shape	$^{+14.7\%}_{-14.8\%}$	$^{+4.5\%}_{-6.9\%}$	$^{+11.4\%}_{-10.9\%}$	$^{+0.0\%}_{-1.5\%}$	$^{+9.1\%}_{-8.9\%}$	$^{+2.7\%}_{-2.9\%}$
ISR/FSR variation	$^{+14.0\%}_{-13.3\%}$	$^{+0.0\%}_{-2.3\%}$	$^{+11.9\%}_{-11.3\%}$	$^{+3.4\%}_{-3.3\%}$	$^{+9.0\%}_{-8.6\%}$	$^{+2.3\%}_{-1.8\%}$
JER	$^{+14.0\%}_{-13.1\%}$	$^{+0.0\%}_{-0.0\%}$	$^{+11.4\%}_{-10.8\%}$	$^{+0.0\%}_{-0.0\%}$	$^{+8.8\%}_{-8.4\%}$	$^{+1.3\%}_{-0.0\%}$
PDF uncertainty	$^{+14.0\%}_{-13.1\%}$	$^{+0.0\%}_{-0.0\%}$	$^{+11.4\%}_{-10.9\%}$	$^{+0.0\%}_{-1.5\%}$	$^{+8.7\%}_{-8.5\%}$	$^{+0.0\%}_{-1.3\%}$
Total	$^{+26.6\%}_{-22.2\%}$	$^{+22.6\%}_{-17.9\%}$	$^{+25.3\%}_{-20.9\%}$	$^{+22.6\%}_{-17.9\%}$	$^{+23.5\%}_{-19.3\%}$	$^{+21.8\%}_{-17.4\%}$

jets. Good agreement is found between the data and the sum of the signal and background derived from the simulation scaled to the fit results. The reduced χ^2 value from a fit of the data to the simulation is 1.8 (0.7) in the electron + jets (muon + jets) channel.

6.6 Cross-checks

To test the robustness of the result, the $t\bar{t}$ cross section is also determined in the muon + jets channel using four additional methods. In the first method, we use a procedure based on counting the number of events with an isolated muon and four or more jets. This method uses an event selection slightly different from that described above. Specifically, the jet p_T is required to be greater than 25 GeV instead of 30 GeV, and the muon is required to have relative isolation less than 0.1, compared to 0.05 in the nominal selection. Also the backgrounds from W/Z + jets and QCD multijet events are calculated by using the technique of Berends scaling [51]. In the second method, we measure the $t\bar{t}$ cross section using a simultaneous fit to the distributions of jet multiplicity (N_{jets}) and the muon transverse momentum, ${p_T}^{\mu}$. The jet multiplicity has been shown (Table 1) to be a powerful variable for separating top from QCD multijet and W + jets events. The variable ${p_T}^{\mu}$ is an attractive choice because it is not directly affected by such systematics as the JES and JER uncertainties. Furthermore, because the muon in either W or $t\bar{t}$ production comes from a W decay, it receives a significant contribution to its momentum from the W rest mass, while muons from QCD multijet events receive no such boost. In the third method, the $t\bar{t}$ cross section is determined from a fit to the muon pseudorapidity distribution in order to separate the top signal from the W + jets and QCD multijet backgrounds. This analysis uses the asymmetry between inclusive W^+ boson and W^- boson production, caused by the difference of the quark charges in the initial-state protons, to determine the templates for the W + jets background. A fourth method measures the $t\bar{t}$ cross section from events containing a high-p_T isolated muon and at least three jets. For this analysis, we relax the relative isolation requirement to $I_{\text{rel}} < 0.1$ but introduce a requirement that the $\not\!\!E_T$ in the event is greater than 20 GeV, in order to keep the amount of QCD multijet background small. A method based on Refs. [52, 53] is used to estimate the amount of QCD multijet background separately for events with three jets and events with at least four jets. The number of top-pair and W + jets events is extracted from a fit to the M3 distribution. All four of these methods give results consistent with our previously quoted measurement, but with slightly larger combined statistical and systematic uncertainties in each case.

Complementary to the top-quark-pair production measurements, the cross section for the production of exactly one muon in association with additional hard jets is measured. In all processes considered as signal for this measurement, the muon originates from a W boson. Both sin-

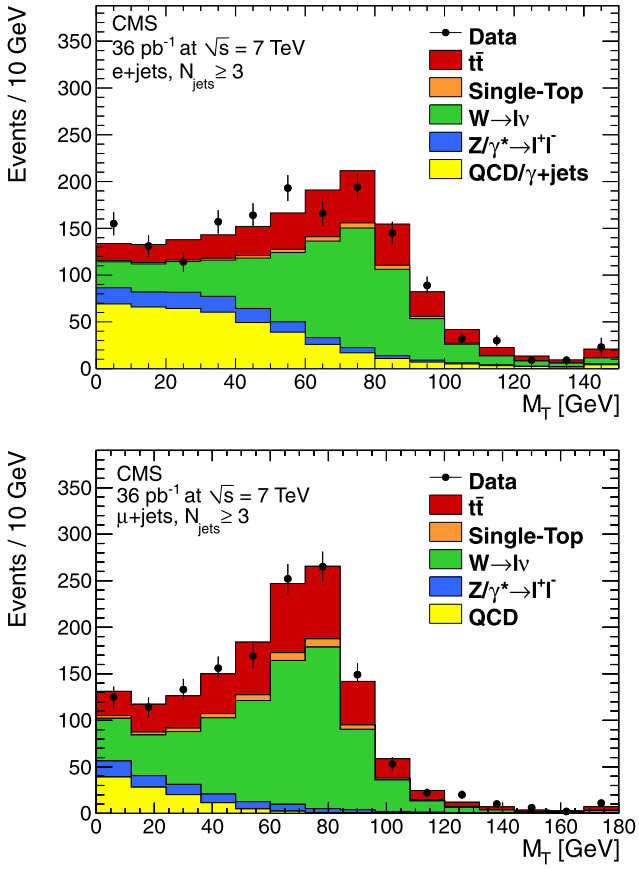

Fig. 7 Transverse mass (M_T) distributions from data and simulation (scaled to the fit results) for (*top*) electron + jets and (*bottom*) muon + jets inclusive three-jet samples

gle top quark decays and decays of top-quark pairs in the lepton + jets channel, including decays via tau leptons in the intermediate state, are contributors to this signature. An additional component of this signal comes from the production of a W boson with additional jets, which is the most prominent background for the analysis of $t\bar{t}$ "lepton + jets" decays. The same event selection as described in Sect. 6.4 is applied. In addition, all jets in data are corrected for pileup, leading to reduced JES and pileup uncertainties. To obtain the cross section, the observed number of events in data is corrected for the remaining background processes. These include QCD multijet production, the production of a Z boson with additional jets, single-top-quark decays, and other $t\bar{t}$ decays. The number of QCD multijet events is determined from data using a template fit to the missing-transverse-energy distribution in each inclusive (or exclusive) jet-multiplicity bin. The normalization and shape of the other backgrounds is taken from the simulation. Figure 8 shows the cross section for the production of a single muon with $p_T > 20$ GeV and $|\eta| < 2.1$ and additional jets as a function of the inclusive and exclusive multiplicity of jets with $p_T > 30$ GeV within $|\eta| < 2.4$. The transition from a phase space dominated by W + jets events (in the 1-jet and 2-jet bins) towards a region dominated by the production of top-quark pairs (in the 4-jet bin) is clearly visible. The comparison of data and simulation indicates a good understanding of this transition, while the overall normalization seems to be slightly underestimated. This is consistent with the main analysis, which also found a W + jets cross section larger than the theoretical prediction.

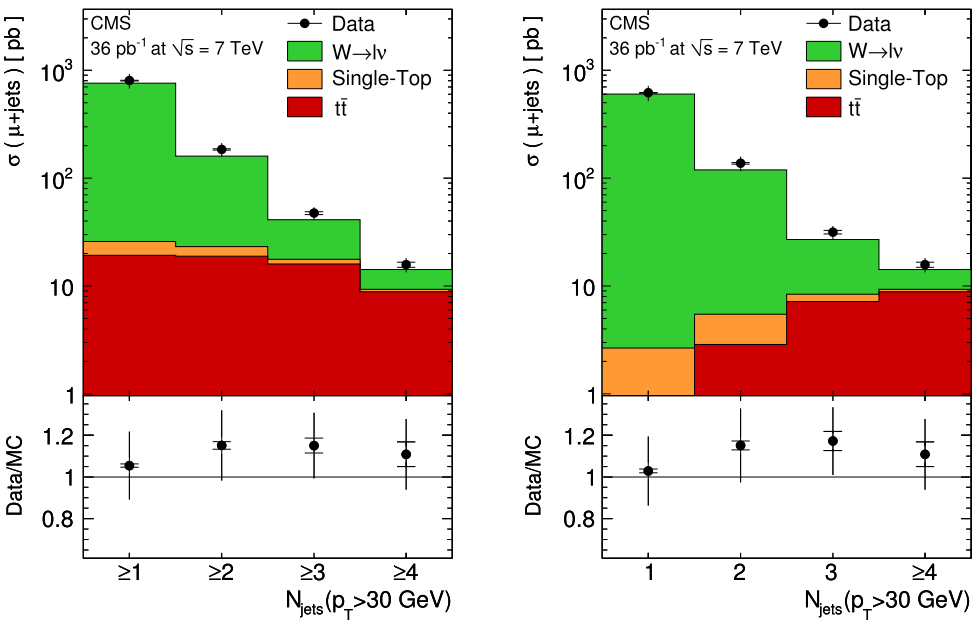

Fig. 8 Cross section for the production of an isolated muon originating from a W boson (including decays via tau leptons in the intermediate state) in association with additional hard jets as a function of the (*left*) inclusive and the (*right*) exclusive multiplicity N_{jets} of jets with $p_T > 30$ GeV in the visible range of the detector. The inner error bars on the data points correspond to the statistical uncertainties while the full error bars correspond to the statistical and systematic uncertainties added in quadrature. The data points are compared with the expectation from the event generators used for the simulation. The scaling factors derived in the main analysis are not applied

7 Discussion and conclusion

A measurement of the cross section for top-quark pair production in proton-proton collisions at a center-of-mass energy of 7 TeV has been performed at the LHC with the CMS detector. The analysis uses a data sample corresponding to an integrated luminosity of 36 pb^{-1} and is based on the reconstruction of final states containing one isolated, high transverse-momentum muon or electron and hadronic jets. The measured cross section for the combined electron + jets and muon + jets channels is $173^{+39}_{-32}\,(\text{stat.} + \text{syst.}) \pm 7\,(\text{lumi.})$ pb. This measurement agrees with but has a larger uncertainty than current theoretical values [10–12, 33, 34], which agree among themselves. For example, the approximate NNLO calculation from Ref. [12] yields $163^{+7}_{-5}\,(\text{scale}) \pm 9\,(\text{PDF})$ pb, while a similar calculation performed using HATHOR [10, 11] yields $160^{+5}_{-9}\,(\text{scale}) \pm 9\,(\text{PDF})$ pb. For this calculation, $Q^2 = (173\ \text{GeV})^2$ is chosen for both the factorization and renormalization scales and the MSTW2008 NNLO [35] PDF set is used. The scale uncertainty is evaluated by independently varying the scales by factors of 4 and 0.25, and the PDF uncertainty is calculated using the 90% confidence level envelope of the PDF [10, 11]. Our cross section measurement also agrees with the earlier CMS measurement in the dilepton channel [14] and the ATLAS measurement in the combined dilepton and lepton + jets channels [15], but has a smaller uncertainty than either of these previous results. Given the agreement between theory and the experimental measurements in both the dilepton and lepton + jets channels, no sign of new physics has emerged in these studies, and the top quark at the LHC remains consistent with being a very massive particle whose properties are as predicted by the standard model.

Acknowledgements We wish to congratulate our colleagues in the CERN accelerator departments for the excellent performance of the LHC machine. We thank the technical and administrative staff at CERN and other CMS institutes. The cost of the detectors, computing infrastructure, data acquisition and all other systems without which CMS would not be able to operate was supported by the financing agencies involved in the experiment. We are particularly indebted to: the Austrian Federal Ministry of Science and Research; the Belgium Fonds de la Recherche Scientifique, and Fonds voor Wetenschappelijk Onderzoek; the Brazilian Funding Agencies (CNPq, CAPES, FAPERJ, and FAPESP); the Bulgarian Ministry of Education and Science; CERN; the Chinese Academy of Sciences, Ministry of Science and Technology, and National Natural Science Foundation of China; the Colombian Funding Agency (COLCIENCIAS); the Croatian Ministry of Science, Education and Sport; the Research Promotion Foundation, Cyprus; the Estonian Academy of Sciences and NICPB; the Academy of Finland, Finnish Ministry of Education, and Helsinki Institute of Physics; the Institut National de Physique Nucléaire et de Physique des Particules/CNRS, and Commissariat à l'Énergie Atomique et aux Énergies Alternatives/CEA, France; the Bundesministerium für Bildung und Forschung, Deutsche Forschungsgemeinschaft, and Helmholtz-Gemeinschaft Deutscher Forschungszentren, Germany; the General Secretariat for Research and Technology, Greece; the National Scientific Research Foundation, and National Office for Research and Technology, Hungary; the Department of Atomic Energy, and Department of Science and Technology, India; the Institute for Studies in Theoretical Physics and Mathematics, Iran; the Science Foundation, Ireland; the Istituto Nazionale di Fisica Nucleare, Italy; the Korean Ministry of Education, Science and Technology and the World Class University program of NRF, Korea; the Lithuanian Academy of Sciences; the Mexican Funding Agencies (CINVESTAV, CONACYT, SEP, and UASLP-FAI); the Pakistan Atomic Energy Commission; the State Commission for Scientific Research, Poland; the Fundação para a Ciência e a Tecnologia, Portugal; JINR (Armenia, Belarus, Georgia, Ukraine, Uzbekistan); the Ministry of Science and Technologies of the Russian Federation, and Russian Ministry of Atomic Energy; the Ministry of Science and Technological Development of Serbia; the Ministerio de Ciencia e Innovación, and Programa Consolider-Ingenio 2010, Spain; the Swiss Funding Agencies (ETH Board, ETH Zurich, PSI, SNF, UniZH, Canton Zurich, and SER); the National Science Council, Taipei; the Scientific and Technical Research Council of Turkey, and Turkish Atomic Energy Authority; the Science and Technology Facilities Council, UK; the US Department of Energy, and the US National Science Foundation.

Individuals have received support from the Marie-Curie programme and the European Research Council (European Union); the Leventis Foundation; the A.P. Sloan Foundation; the Alexander von Humboldt Foundation; the Associazione per lo Sviluppo Scientifico e Tecnologico del Piemonte (Italy); the Belgian Federal Science Policy Office; the Fonds pour la Formation à la Recherche dans l'Industrie et dans l'Agriculture (FRIA-Belgium); and the Agentschap voor Innovatie door Wetenschap en Technologie (IWT-Belgium).

References

1. J.R. Incandela et al., Status and prospects of top-quark physics. Prog. Part. Nucl. Phys. **63**, 239 (2009). arXiv:0904.2499, doi:10.1016/j.ppnp.2009.08.001
2. CDF Collaboration, Observation of top quark production in $\bar{\text{p}}\text{p}$ collisions. Phys. Rev. Lett. **74**, 2626 (1995). arXiv:hep-ex/9503002, doi:10.1103/PhysRevLett.74.2626
3. D0 Collaboration, Observation of the top quark. Phys. Rev. Lett. **74**, 2632 (1995). arXiv:hep-ex/9503003, doi:10.1103/PhysRevLett.74.2632
4. L. Evans, P. Bryant (eds.), LHC machine. J. Instrum. **03**, S08001 (2008). doi:10.1088/1748-0221/3/08/S08001
5. W. Bernreuther et al., Top quark spin correlations at hadron colliders: predictions at next-to-leading order QCD. Phys. Rev. Lett. **87**, 242002 (2001). arXiv:hep-ph/0107086, doi:10.1103/PhysRevLett.87.242002
6. W. Bernreuther et al., Top quark pair production and decay at hadron colliders. Nucl. Phys. B **690**, 81 (2004). arXiv:hep-ph/0403035, doi:10.1016/j.nuclphysb.2004.04.019
7. P. Nason, S. Dawson, R. Ellis, The total cross-section for the production of heavy quarks in hadronic collisions. Nucl. Phys. B **303**, 607 (1988). doi:10.1016/0550-3213(88)90422-1
8. W. Beenakker et al., QCD corrections to heavy quark production in $\text{p}\bar{\text{p}}$ collisions. Phys. Rev. D **40**, 54 (1989). doi:10.1103/PhysRevD.40.54
9. M. Czakon, A. Mitov, Inclusive heavy flavor hadroproduction in NLO QCD: the exact analytic result. Nucl. Phys. B **824**, 111 (2010). arXiv:0811.4119, doi:10.1016/j.nuclphysb.2009.08.020

10. M. Aliev et al., HATHOR: HAdronic Top and Heavy quarks crOss section calculatoR. Comput. Phys. Commun. **182**, 1034 (2011). arXiv:1007.1327, doi:10.1016/j.cpc.2010.12.040
11. U. Langenfeld, S. Moch, P. Uwer, Measuring the running top-quark mass. Phys. Rev. D **80**, 054009 (2009). arXiv:0906.5273, doi:10.1103/PhysRevD.80.054009
12. N. Kidonakis, Next-to-next-to-leading soft-gluon corrections for the top quark cross section and transverse momentum distribution. Phys. Rev. D **82**, 114030 (2010). arXiv:1009.4935, doi:10.1103/PhysRevD.82.114030
13. M. Cacciari et al., Updated predictions for the total production cross sections of top and of heavier quark pairs at the Tevatron and at the LHC. J. High Energy Phys. **09**, 127 (2008). arXiv:0804.2800, doi:10.1088/1126-6708/2008/09/127
14. CMS Collaboration, First measurement of the cross section for top-quark pair production in proton-proton collisions at $\sqrt{s} =$ 7 TeV. Phys. Lett. B **695**, 424 (2011). arXiv:1010.5994, doi:10.1016/j.physletb.2010.11.058
15. ATLAS Collaboration, Measurement of the top quark-pair production cross section with ATLAS in pp collisions at $\sqrt{s} =$ 7 TeV. Eur. Phys. J. C **71**, 1577 (2011). doi:10.1140/epjc/s10052-011-1577-6
16. CMS Collaboration, The CMS experiment at the CERN LHC. J. Instrum. **03**, S08004 (2008). doi:10.1088/1748-0221/3/08/S08004
17. S. Baffioni et al., Electron reconstruction in CMS. Eur. Phys. J. C **49**, 1099 (2007). doi:10.1140/epjc/s10052-006-0175-5
18. CMS Collaboration, Electron reconstruction and identification at $\sqrt{s} = 7$ TeV. CMS Physics Analysis Summary **EGM-10-004** (2010). http://cdsweb.cern.ch/record/1299116
19. CMS Collaboration, Performance of muon identification in pp collisions at $\sqrt{s} = 7$ TeV. CMS Physics Analysis Summary **MUO-10-002** (2010). http://cdsweb.cern.ch/record/1279140
20. CMS Collaboration, Measurement of the charge ratio of atmospheric muons with the CMS detector. Phys. Lett. B **692**, 83 (2010). arXiv:1005.5332, doi:10.1016/j.physletb.2010.07.033
21. CMS Collaboration, Particle-flow event reconstruction in CMS and performance for jets, taus, and missing E_{T}. CMS Physics Analysis Summary **PFT-09-001** (2009). http://cdsweb.cern.ch/record/1194487
22. CMS Collaboration, Commissioning of the particle-flow reconstruction in minimum-bias and jet events from pp collisions at 7 TeV. CMS Physics Analysis Summary **PFT-10-002** (2010). http://cdsweb.cern.ch/record/1279341
23. CMS Collaboration, Jet performance in pp collisions at $\sqrt{s} =$ 7 TeV. CMS Physics Analysis Summary **JME-10-003** (2010). http://cdsweb.cern.ch/record/1279347
24. M. Cacciari, G.P. Salam, G. Soyez, The anti-k_t jet clustering algorithm. J. High Energy Phys. **04**, 063 (2008). arXiv:0802.1189, doi:10.1088/1126-6708/2008/04/063
25. M. Cacciari, G.P. Salam, Dispelling the N^3 myth for the k_t jet-finder. Phys. Lett. B **641**, 57 (2006). arXiv:hep-ph/0512210, doi:10.1016/j.physletb.2006.08.037
26. J. Allison et al., Geant4 developments and applications. IEEE Trans. Nucl. Sci. **53**, 270 (2006). doi:10.1109/TNS.2006.869826
27. CMS Collaboration, Measurement of CMS luminosity. CMS Physics Analysis Summary **CMS-PAS-EWK-10-004** (2010). http://cdsweb.cern.ch/record/1279145
28. CMS Collaboration, Absolute luminosity normalization. CMS Detector Performance Summary **DP-2011-003** (2011). http://cdsweb.cern.ch/record/1335668
29. CMS Collaboration, CMS tracking performance results from early LHC operation. Eur. Phys. J. C **70**, 1165 (2010). arXiv:1007.1988, doi:10.1140/epjc/s10052-010-1491-3
30. J. Alwall et al., MadGraph/MadEvent v4: the new web generation. J. High Energy Phys. **09**, 028 (2007). arXiv:0706.2334, doi:10.1088/1126-6708/2007/09/028
31. T. Sjöstrand, S. Mrenna, P.Z. Skands, PYTHIA 6.4 physics and manual. J. High Energy Phys. **05**, 026 (2006). arXiv:hep-ph/0603175, doi:10.1088/1126-6708/2006/05/026
32. M.L. Mangano et al., Matching matrix elements and shower evolution for top-quark production in hadronic collisions. J. High Energy Phys. **01**, 013 (2007). arXiv:hep-ph/0611129, doi:10.1088/1126-6708/2007/01/013
33. J.M. Campbell, R.K. Ellis, Radiative corrections to Z b anti-b production. Phys. Rev. D **62**, 114012 (2000). arXiv:hep-ph/0006304, doi:10.1103/PhysRevD.62.114012
34. R. Kleiss, W.J. Stirling, Top quark production at hadron colliders: some useful formulae. Z. Phys. C **40**, 419 (1988). doi:10.1007/BF01548856
35. A.D. Martin et al., Uncertainties on α_S in global PDF analyses and implications for predicted hadronic cross sections. Eur. Phys. J. C **64**, 653 (2009). arXiv:0905.3531, doi:10.1140/epjc/s10052-009-1164-2
36. CTEQ Collaboration, Uncertainty induced by QCD coupling in the CTEQ global analysis of parton distributions (2010). arXiv:1004.4624
37. F. Demartin et al., The impact of PDF and α_S uncertainties on Higgs production in gluon fusion at hadron colliders. Phys. Rev. D **82**, 014002 (2010). arXiv:1004.0962, doi:10.1103/PhysRevD.82.014002
38. PDF4LHC Collaboration, The PDF4LHC working group interim recommendations (2011). arXiv:1101.0538
39. J.M. Campbell et al., Next-to-leading-order predictions for t-channel single-top production at hadron colliders. Phys. Rev. Lett. **102**, 182003 (2009). arXiv:0903.0005, doi:10.1103/PhysRevLett.102.182003
40. J.M. Campbell, F. Tramontano, Next-to-leading order corrections to W t production and decay. Nucl. Phys. B **726**, 109 (2005). arXiv:hep-ph/0506289, doi:10.1016/j.nuclphysb.2005.08.015
41. J.M. Campbell, R.K. Ellis, F. Tramontano, Single top production and decay at next-to-leading order. Phys. Rev. D **70**, 094012 (2004). arXiv:hep-ph/0408158, doi:10.1103/PhysRevD.70.094012
42. K. Melnikov, F. Petriello, Electroweak gauge boson production at hadron colliders through $O(\alpha_s^2)$. Phys. Rev. D **74**, 114017 (2006). arXiv:hep-ph/0609070, doi:10.1103/PhysRevD.74.114017
43. CMS Collaboration, Measurement of the single-top t-channel cross section in pp collisions at $\sqrt{s} = 7$ TeV. CMS Physics Analysis Summary **TOP-10-008** (2011). http://cdsweb.cern.ch/record/1335719
44. CMS Collaboration, Rates of jets produced in association with W and Z bosons in pp collisions at $\sqrt{s} = 7$ TeV. CMS Physics Analysis Summary **EWK-10-012** (2011). http://cdsweb.cern.ch/record/1337018
45. J. Neyman, Outline of a theory of statistical estimation based on the classical theory of probability. Philos. Trans. R. Soc. Lond. Ser. A, Math. Phys. Sci. **236**(767), 333 (1937). doi:10.1098/rsta.1937.0005
46. CMS Collaboration, Determination of the jet energy scale in CMS with pp collisions at $\sqrt{s} = 7$ TeV. CMS Physics Analysis Summary **JME-10-010** (2010). http://cdsweb.cern.ch/record/1308178
47. G. Corcella et al., HERWIG 6.5: an event generator for hadron emission reactions with interfering gluons (including supersymmetric processes). J. High Energy Phys. **01**, 010 (2001). arXiv:hep-ph/0011363
48. CMS Collaboration, Jet resolution in CMS at $\sqrt{s} = 7$ TeV. CMS Physics Analysis Summary **JME-10-014** (2010). http://cdsweb.cern.ch/record/1339945
49. P.M. Nadolsky et al., Implications of CTEQ global analysis for collider observables. Phys. Rev. D **78**, 013004 (2008). arXiv:0802.0007, doi:10.1103/PhysRevD.78.013004

50. WBG Collaboration, The Les Houches accord PDFs (LHAPDF) and Lhaglue (2005). arXiv:hep-ph/0508110
51. F.A. Berends et al., On the production of a W and jets at hadron colliders. Nucl. Phys. B **357**, 32 (1991). doi:10.1016/0550-3213(91)90458-A
52. D0 Collaboration, Measurement of the $t\bar{t}$ production cross section in $p\bar{p}$ collisions at $\sqrt{s} = 1.96$ TeV using secondary vertex b tagging. Phys. Rev. D **74**, 112004 (2006). arXiv:hep-ex/0611002, doi:10.1103/PhysRevD.74.112004
53. R.J. Barlow, Event classification using weighting methods. J. Comput. Phys. **72**, 202 (1987). doi:10.1016/0021-9991(87)90078-7

The CMS Collaboration

Yerevan Physics Institute, Yerevan, Armenia
S. Chatrchyan, V. Khachatryan, A.M. Sirunyan, A. Tumasyan

Institut für Hochenergiephysik der OeAW, Wien, Austria
W. Adam, T. Bergauer, M. Dragicevic, J. Erö, C. Fabjan, M. Friedl, R. Frühwirth, V.M. Ghete, J. Hammer[1], S. Hänsel, M. Hoch, N. Hörmann, J. Hrubec, M. Jeitler, W. Kiesenhofer, M. Krammer, D. Liko, I. Mikulec, M. Pernicka, H. Rohringer, R. Schöfbeck, J. Strauss, A. Taurok, F. Teischinger, P. Wagner, W. Waltenberger, G. Walzel, E. Widl, C.-E. Wulz

National Centre for Particle and High Energy Physics, Minsk, Belarus
V. Mossolov, N. Shumeiko, J. Suarez Gonzalez

Universiteit Antwerpen, Antwerpen, Belgium
S. Bansal, L. Benucci, E.A. De Wolf, X. Janssen, J. Maes, T. Maes, L. Mucibello, S. Ochesanu, B. Roland, R. Rougny, M. Selvaggi, H. Van Haevermaet, P. Van Mechelen, N. Van Remortel

Vrije Universiteit Brussel, Brussel, Belgium
F. Blekman, S. Blyweert, J. D'Hondt, O. Devroede, R. Gonzalez Suarez, A. Kalogeropoulos, M. Maes, W. Van Doninck, P. Van Mulders, G.P. Van Onsem, I. Villella

Université Libre de Bruxelles, Bruxelles, Belgium
O. Charaf, B. Clerbaux, G. De Lentdecker, V. Dero, A.P.R. Gay, G.H. Hammad, T. Hreus, P.E. Marage, L. Thomas, C. Vander Velde, P. Vanlaer

Ghent University, Ghent, Belgium
V. Adler, A. Cimmino, S. Costantini, M. Grunewald, B. Klein, J. Lellouch, A. Marinov, J. Mccartin, D. Ryckbosch, F. Thyssen, M. Tytgat, L. Vanelderen, P. Verwilligen, S. Walsh, N. Zaganidis

Université Catholique de Louvain, Louvain-la-Neuve, Belgium
S. Basegmez, G. Bruno, J. Caudron, L. Ceard, E. Cortina Gil, J. De Favereau De Jeneret, C. Delaere[1], D. Favart, A. Giammanco, G. Grégoire, J. Hollar, V. Lemaitre, J. Liao, O. Militaru, S. Ovyn, D. Pagano, A. Pin, K. Piotrzkowski, N. Schul

Université de Mons, Mons, Belgium
N. Beliy, T. Caebergs, E. Daubie

Centro Brasileiro de Pesquisas Fisicas, Rio de Janeiro, Brazil
G.A. Alves, D. De Jesus Damiao, M.E. Pol, M.H.G. Souza

Universidade do Estado do Rio de Janeiro, Rio de Janeiro, Brazil
W. Carvalho, E.M. Da Costa, C. De Oliveira Martins, S. Fonseca De Souza, L. Mundim, H. Nogima, V. Oguri, W.L. Prado Da Silva, A. Santoro, S.M. Silva Do Amaral, A. Sznajder

Instituto de Fisica Teorica, Universidade Estadual Paulista, Sao Paulo, Brazil
C.A. Bernardes[2], F.A. Dias, T.R. Fernandez Perez Tomei, E.M. Gregores[2], C. Lagana, F. Marinho, P.G. Mercadante[2], S.F. Novaes, S.S. Padula

Institute for Nuclear Research and Nuclear Energy, Sofia, Bulgaria
N. Darmenov[1], V. Genchev[1], P. Iaydjiev[1], S. Piperov, M. Rodozov, S. Stoykova, G. Sultanov, V. Tcholakov, R. Trayanov

University of Sofia, Sofia, Bulgaria
A. Dimitrov, R. Hadjiiska, A. Karadzhinova, V. Kozhuharov, L. Litov, M. Mateev, B. Pavlov, P. Petkov

Institute of High Energy Physics, Beijing, China
J.G. Bian, G.M. Chen, H.S. Chen, C.H. Jiang, D. Liang, S. Liang, X. Meng, J. Tao, J. Wang, J. Wang, X. Wang, Z. Wang, H. Xiao, M. Xu, J. Zang, Z. Zhang

State Key Lab. of Nucl. Phys. and Tech., Peking University, Beijing, China
Y. Ban, S. Guo, Y. Guo, W. Li, Y. Mao, S.J. Qian, H. Teng, B. Zhu, W. Zou

Universidad de Los Andes, Bogota, Colombia
A. Cabrera, B. Gomez Moreno, A.A. Ocampo Rios, A.F. Osorio Oliveros, J.C. Sanabria

Technical University of Split, Split, Croatia
N. Godinovic, D. Lelas, K. Lelas, R. Plestina[3], D. Polic, I. Puljak

University of Split, Split, Croatia
Z. Antunovic, M. Dzelalija

Institute Rudjer Boskovic, Zagreb, Croatia
V. Brigljevic, S. Duric, K. Kadija, S. Morovic

University of Cyprus, Nicosia, Cyprus
A. Attikis, M. Galanti, J. Mousa, C. Nicolaou, F. Ptochos, P.A. Razis

Charles University, Prague, Czech Republic
M. Finger, M. Finger Jr.

Academy of Scientific Research and Technology of the Arab Republic of Egypt, Egyptian Network of High Energy Physics, Cairo, Egypt
Y. Assran[4], S. Khali[5], M.A. Mahmoud[6]

National Institute of Chemical Physics and Biophysics, Tallinn, Estonia
A. Hektor, M. Kadastik, M. Müntel, M. Raidal, L. Rebane

Department of Physics, University of Helsinki, Helsinki, Finland
V. Azzolini, P. Eerola, G. Fedi

Helsinki Institute of Physics, Helsinki, Finland
S. Czellar, J. Härkönen, A. Heikkinen, V. Karimäki, R. Kinnunen, M.J. Kortelainen, T. Lampén, K. Lassila-Perini, S. Lehti, T. Lindén, P. Luukka, T. Mäenpää, E. Tuominen, J. Tuominiemi, E. Tuovinen, D. Ungaro, L. Wendland

Lappeenranta University of Technology, Lappeenranta, Finland
K. Banzuzi, A. Korpela, T. Tuuva

Laboratoire d'Annecy-le-Vieux de Physique des Particules, IN2P3-CNRS, Annecy-le-Vieux, France
D. Sillou

DSM/IRFU, CEA/Saclay, Gif-sur-Yvette, France
M. Besancon, S. Choudhury, M. Dejardin, D. Denegri, B. Fabbro, J.L. Faure, F. Ferri, S. Ganjour, F.X. Gentit, A. Givernaud, P. Gras, G. Hamel de Monchenault, P. Jarry, E. Locci, J. Malcles, M. Marionneau, L. Millischer, J. Rander, A. Rosowsky, I. Shreyber, M. Titov, P. Verrecchia

Laboratoire Leprince-Ringuet, Ecole Polytechnique, IN2P3-CNRS, Palaiseau, France
S. Baffioni, F. Beaudette, L. Benhabib, L. Bianchini, M. Bluj[7], C. Broutin, P. Busson, C. Charlot, T. Dahms, L. Dobrzynski, S. Elgammal, R. Granier de Cassagnac, M. Haguenauer, P. Miné, C. Mironov, C. Ochando, P. Paganini, D. Sabes, R. Salerno, Y. Sirois, C. Thiebaux, B. Wyslouch[8], A. Zabi

Institut Pluridisciplinaire Hubert Curien, Université de Strasbourg, Université de Haute Alsace Mulhouse, CNRS/IN2P3, Strasbourg, France
J.-L. Agram[9], J. Andrea, D. Bloch, D. Bodin, J.-M. Brom, M. Cardaci, E.C. Chabert, C. Collard, E. Conte[9], F. Drouhin[9], C. Ferro, J.-C. Fontaine[9], D. Gelé, U. Goerlach, S. Greder, P. Juillot, M. Karim[9], A.-C. Le Bihan, Y. Mikami, P. Van Hove

Centre de Calcul de l'Institut National de Physique Nucleaire et de Physique des Particules (IN2P3), Villeurbanne, France
F. Fassi, D. Mercier

Université de Lyon, Université Claude Bernard Lyon 1, CNRS-IN2P3, Institut de Physique Nucléaire de Lyon, Villeurbanne, France
C. Baty, S. Beauceron, N. Beaupere, M. Bedjidian, O. Bondu, G. Boudoul, D. Boumediene, H. Brun, J. Chasserat, R. Chierici, D. Contardo, P. Depasse, H. El Mamouni, J. Fay, S. Gascon, B. Ille, T. Kurca, T. Le Grand, M. Lethuillier, L. Mirabito, S. Perries, V. Sordini, S. Tosi, Y. Tschudi, P. Verdier

Institute of High Energy Physics and Informatization, Tbilisi State University, Tbilisi, Georgia
D. Lomidze

RWTH Aachen University, I. Physikalisches Institut, Aachen, Germany
G. Anagnostou, M. Edelhoff, L. Feld, N. Heracleous, O. Hindrichs, R. Jussen, K. Klein, J. Merz, N. Mohr, A. Ostapchuk, A. Perieanu, F. Raupach, J. Sammet, S. Schael, D. Sprenger, H. Weber, M. Weber, B. Wittmer

RWTH Aachen University, III. Physikalisches Institut A, Aachen, Germany
M. Ata, W. Bender, E. Dietz-Laursonn, M. Erdmann, J. Frangenheim, T. Hebbeker, A. Hinzmann, K. Hoepfner, T. Klimkovich, D. Klingebiel, P. Kreuzer, D. Lanske[†], C. Magass, M. Merschmeyer, A. Meyer, P. Papacz, H. Pieta, H. Reithler, S.A. Schmitz, L. Sonnenschein, J. Steggemann, D. Teyssier

RWTH Aachen University, III. Physikalisches Institut B, Aachen, Germany
M. Bontenackels, M. Davids, M. Duda, G. Flügge, H. Geenen, M. Giffels, W. Haj Ahmad, D. Heydhausen, T. Kress, Y. Kuessel, A. Linn, A. Nowack, L. Perchalla, O. Pooth, J. Rennefeld, P. Sauerland, A. Stahl, M. Thomas, D. Tornier, M.H. Zoeller

Deutsches Elektronen-Synchrotron, Hamburg, Germany
M. Aldaya Martin, W. Behrenhoff, U. Behrens, M. Bergholz[10], A. Bethani, K. Borras, A. Cakir, A. Campbell, E. Castro, D. Dammann, G. Eckerlin, D. Eckstein, A. Flossdorf, G. Flucke, A. Geiser, J. Hauk, H. Jung[1], M. Kasemann, I. Katkov[11], P. Katsas, C. Kleinwort, H. Kluge, A. Knutsson, M. Krämer, D. Krücker, E. Kuznetsova, W. Lange, W. Lohmann[10], R. Mankel, M. Marienfeld, I.-A. Melzer-Pellmann, A.B. Meyer, J. Mnich, A. Mussgiller, J. Olzem, A. Petrukhin, D. Pitzl, A. Raspereza, A. Raval, M. Rosin, R. Schmidt[10], T. Schoerner-Sadenius, N. Sen, A. Spiridonov, M. Stein, J. Tomaszewska, R. Walsh, C. Wissing

University of Hamburg, Hamburg, Germany
C. Autermann, V. Blobel, S. Bobrovskyi, J. Draeger, H. Enderle, U. Gebbert, M. Görner, K. Kaschube, G. Kaussen, R. Klanner, J. Lange, B. Mura, S. Naumann-Emme, F. Nowak, N. Pietsch, C. Sander, H. Schettler, P. Schleper, E. Schlieckau, M. Schröder, T. Schum, J. Schwandt, H. Stadie, G. Steinbrück, J. Thomsen

Institut für Experimentelle Kernphysik, Karlsruhe, Germany
C. Barth, J. Bauer, J. Berger, V. Buege, T. Chwalek, W. De Boer, A. Dierlamm, G. Dirkes, M. Feindt, J. Gruschke, C. Hackstein, F. Hartmann, M. Heinrich, H. Held, K.H. Hoffmann, S. Honc, J.R. Komaragiri, T. Kuhr, D. Martschei, S. Mueller, Th. Müller, M. Niegel, O. Oberst, A. Oehler, J. Ott, T. Peiffer, G. Quast, K. Rabbertz, F. Ratnikov, N. Ratnikova, M. Renz, C. Saout, A. Scheurer, P. Schieferdecker, F.-P. Schilling, G. Schott, H.J. Simonis, F.M. Stober, D. Troendle, J. Wagner-Kuhr, T. Weiler, M. Zeise, V. Zhukov[11], E.B. Ziebarth

Institute of Nuclear Physics "Demokritos", Aghia Paraskevi, Greece
G. Daskalakis, T. Geralis, S. Kesisoglou, A. Kyriakis, D. Loukas, I. Manolakos, A. Markou, C. Markou, C. Mavrommatis, E. Ntomari, E. Petrakou

University of Athens, Athens, Greece
L. Gouskos, T.J. Mertzimekis, A. Panagiotou, E. Stiliaris

University of Ioánnina, Ioánnina, Greece
I. Evangelou, C. Foudas, P. Kokkas, N. Manthos, I. Papadopoulos, V. Patras, F.A. Triantis

KFKI Research Institute for Particle and Nuclear Physics, Budapest, Hungary
A. Aranyi, G. Bencze, L. Boldizsar, C. Hajdu[1], P. Hidas, D. Horvath[12], A. Kapusi, K. Krajczar[13], F. Sikler[1], G.I. Veres[13], G. Vesztergombi[13]

Institute of Nuclear Research ATOMKI, Debrecen, Hungary
N. Beni, J. Molnar, J. Palinkas, Z. Szillasi, V. Veszpremi

University of Debrecen, Debrecen, Hungary
P. Raics, Z.L. Trocsanyi, B. Ujvari

Panjab University, Chandigarh, India
S.B. Beri, V. Bhatnagar, N. Dhingra, R. Gupta, M. Jindal, M. Kaur, J.M. Kohli, M.Z. Mehta, N. Nishu, L.K. Saini, A. Sharma, A.P. Singh, J.B. Singh, S.P. Singh

University of Delhi, Delhi, India
S. Ahuja, S. Bhattacharya, B.C. Choudhary, B. Gomber, P. Gupta, S. Jain, S. Jain, R. Khurana, A. Kumar, M. Naimuddin, K. Ranjan, R.K. Shivpuri

Saha Institute of Nuclear Physics, Kolkata, India
S. Dutta, S. Sarkar

Bhabha Atomic Research Centre, Mumbai, India
R.K. Choudhury, D. Dutta, S. Kailas, V. Kumar, P. Mehta, A.K. Mohanty[1], L.M. Pant, P. Shukla

Tata Institute of Fundamental Research—EHEP, Mumbai, India
T. Aziz, M. Guchait[14], A. Gurtu, M. Maity[15], D. Majumder, G. Majumder, K. Mazumdar, G.B. Mohanty, A. Saha, K. Sudhakar, N. Wickramage

Tata Institute of Fundamental Research—HECR, Mumbai, India
S. Banerjee, S. Dugad, N.K. Mondal

Institute for Research and Fundamental Sciences (IPM), Tehran, Iran
H. Arfaei, H. Bakhshiansohi[16], S.M. Etesami, A. Fahim[16], M. Hashemi, A. Jafari[16], M. Khakzad, A. Mohammadi[17], M. Mohammadi Najafabadi, S. Paktinat Mehdiabadi, B. Safarzadeh, M. Zeinali[18]

INFN Sezione di Bari[a], Università di Bari[b], Politecnico di Bari[c], Bari, Italy
M. Abbrescia[a,b], L. Barbone[a,b], C. Calabria[a,b], A. Colaleo[a], D. Creanza[a,c], N. De Filippis[a,c,1], M. De Palma[a,b], L. Fiore[a], G. Iaselli[a,c], L. Lusito[a,b], G. Maggi[a,c], M. Maggi[a], N. Manna[a,b], B. Marangelli[a,b], S. My[a,c], S. Nuzzo[a,b], N. Pacifico[a,b], G.A. Pierro[a], A. Pompili[a,b], G. Pugliese[a,c], F. Romano[a,c], G. Roselli[a,b], G. Selvaggi[a,b], L. Silvestris[a], R. Trentadue[a], S. Tupputi[a,b], G. Zito[a]

INFN Sezione di Bologna[a], Università di Bologna[b], Bologna, Italy
G. Abbiendi[a], A.C. Benvenuti[a], D. Bonacorsi[a], S. Braibant-Giacomelli[a,b], L. Brigliadori[a], P. Capiluppi[a,b], A. Castro[a,b], F.R. Cavallo[a], M. Cuffiani[a,b], G.M. Dallavalle[a], F. Fabbri[a], A. Fanfani[a,b], D. Fasanella[a], P. Giacomelli[a], M. Giunta[a], C. Grandi[a], S. Marcellini[a], G. Masetti[b], M. Meneghelli[a,b], A. Montanari[a], F.L. Navarria[a,b], F. Odorici[a], A. Perrotta[a], F. Primavera[a], A.M. Rossi[a,b], T. Rovelli[a,b], G. Siroli[a,b], R. Travaglini[a,b]

INFN Sezione di Catania[a], Università di Catania[b], Catania, Italy
S. Albergo[a,b], G. Cappello[a,b], M. Chiorboli[a,b,1], S. Costa[a,b], A. Tricomi[a,b], C. Tuve[a,b]

INFN Sezione di Firenze[a], Università di Firenze[b], Firenze, Italy
G. Barbagli[a], V. Ciulli[a,b], C. Civinini[a], R. D'Alessandro[a,b], E. Focardi[a,b], S. Frosali[a,b], E. Gallo[a], S. Gonzi[a,b], P. Lenzi[a,b], M. Meschini[a], S. Paoletti[a], G. Sguazzoni[a], A. Tropiano[a,1]

INFN Laboratori Nazionali di Frascati, Frascati, Italy
L. Benussi, S. Bianco, S. Colafranceschi[19], F. Fabbri, D. Piccolo

INFN Sezione di Genova, Genova, Italy
P. Fabbricatore, R. Musenich

INFN Sezione di Milano-Biccoca[a], Università di Milano-Bicocca[b], Milano, Italy
A. Benaglia[a,b], F. De Guio[a,b,1], L. Di Matteo[a,b], S. Gennai[1], A. Ghezzi[a,b], S. Malvezzi[a], A. Martelli[a,b], A. Massironi[a,b], D. Menasce[a], L. Moroni[a], M. Paganoni[a,b], D. Pedrini[a], S. Ragazzi[a,b], N. Redaelli[a], S. Sala[a], T. Tabarelli de Fatis[a,b]

INFN Sezione di Napoli[a], Università di Napoli "Federico II"[b], Napoli, Italy
S. Buontempo[a], C.A. Carrillo Montoya[a,1], N. Cavallo[a,20], A. De Cosa[a,b], F. Fabozzi[a,20], A.O.M. Iorio[a,1], L. Lista[a], M. Merola[a,b], P. Paolucci[a]

INFN Sezione di Padova[a], Università di Padova[b], Università di Trento (Trento)[c], Padova, Italy
P. Azzi[a], N. Bacchetta[a], P. Bellan[a,b], D. Bisello[a,b], A. Branca[a], R. Carlin[a,b], P. Checchia[a], M. De Mattia[a,b], T. Dorigo[a], U. Dosselli[a], F. Fanzago[a], F. Gasparini[a,b], U. Gasparini[a,b], A. Gozzelino, S. Lacaprara[a,21], I. Lazzizzera[a,c], M. Margoni[a,b], M. Mazzucato[a], A.T. Meneguzzo[a,b], M. Nespolo[a,1], L. Perrozzi[a,1], N. Pozzobon[a,b], P. Ronchese[a,b], F. Simonetto[a,b], E. Torassa[a], M. Tosi[a,b], S. Vanini[a,b], P. Zotto[a,b], G. Zumerle[a,b]

INFN Sezione di Pavia[a], Università di Pavia[b], Pavia, Italy
P. Baesso[a,b], U. Berzano[a], S.P. Ratti[a,b], C. Riccardi[a,b], P. Torre[a,b], P. Vitulo[a,b], C. Viviani[a,b]

INFN Sezione di Perugia[a], Università di Perugia[b], Perugia, Italy
M. Biasini[a,b], G.M. Bilei[a], B. Caponeri[a,b], L. Fanò[a,b], P. Lariccia[a,b], A. Lucaroni[a,b,1], G. Mantovani[a,b], M. Menichelli[a], A. Nappi[a,b], F. Romeo[a,b], A. Santocchia[a,b], S. Taroni[a,b,1], M. Valdata[a,b]

INFN Sezione di Pisa[a], Università di Pisa[b], Scuola Normale Superiore di Pisa[c], Pisa, Italy
P. Azzurri[a,c], G. Bagliesi[a], J. Bernardini[a,b], T. Boccali[a,1], G. Broccolo[a,c], R. Castaldi[a], R.T. D'Agnolo[a,c], R. Dell'Orso[a], F. Fiori[a,b], L. Foà[a,c], A. Giassi[a], A. Kraan[a], F. Ligabue[a,c], T. Lomtadze[a], L. Martini[a,22], A. Messineo[a,b], F. Palla[a], G. Segneri[a], A.T. Serban[a], P. Spagnolo[a], R. Tenchini[a], G. Tonelli[a,b,1], A. Venturi[a,1], P.G. Verdini[a]

INFN Sezione di Roma[a], Università di Roma "La Sapienza"[b], Roma, Italy
L. Barone[a,b], F. Cavallari[a], D. Del Re[a,b], E. Di Marco[a,b], M. Diemoz[a], D. Franci[a,b], M. Grassi[a,1], E. Longo[a,b], S. Nourbakhsh[a], G. Organtini[a,b], F. Pandolfi[a,b,1], R. Paramatti[a], S. Rahatlou[a,b], C. Roveli[1]

INFN Sezione di Torino[a], Università di Torino[b], Università del Piemonte Orientale (Novara)[c], Torino, Italy
N. Amapane[a,b], R. Arcidiacono[a,c], S. Argiro[a,b], M. Arneodo[a,c], C. Biino[a], C. Botta[a,b,1], N. Cartiglia[a], R. Castello[a,b], M. Costa[a,b], N. Demaria[a], A. Graziano[a,b,1], C. Mariotti[a], M. Marone[a,b], S. Maselli[a], E. Migliore[a,b], G. Mila[a,b], V. Monaco[a,b], M. Musich[a,b], M.M. Obertino[a,c], N. Pastrone[a], M. Pelliccioni[a,b], A. Romero[a,b], M. Ruspa[a,c], R. Sacchi[a,b], V. Sola[a,b], A. Solano[a,b], A. Staiano[a], A. Vilela Pereira[a]

INFN Sezione di Trieste[a], Università di Trieste[b], Trieste, Italy
S. Belforte[a], F. Cossutti[a], G. Della Ricca[a,b], B. Gobbo[a], D. Montanino[a,b], A. Penzo[a]

Kangwon National University, Chunchon, Korea
S.G. Heo, S.K. Nam

Kyungpook National University, Daegu, Korea
S. Chang, J. Chung, D.H. Kim, G.N. Kim, J.E. Kim, D.J. Kong, H. Park, S.R. Ro, D. Son, D.C. Son, T. Son

Chonnam National University, Institute for Universe and Elementary Particles, Kwangju, Korea
Zero Kim, J.Y. Kim, S. Song

Korea University, Seoul, Korea
S. Choi, B. Hong, M.S. Jeong, M. Jo, H. Kim, J.H. Kim, T.J. Kim, K.S. Lee, D.H. Moon, S.K. Park, H.B. Rhee, E. Seo, S. Shin, K.S. Sim

University of Seoul, Seoul, Korea
M. Choi, S. Kang, H. Kim, C. Park, I.C. Park, S. Park, G. Ryu

Sungkyunkwan University, Suwon, Korea
Y. Choi, Y.K. Choi, J. Goh, M.S. Kim, E. Kwon, J. Lee, S. Lee, H. Seo, I. Yu

Vilnius University, Vilnius, Lithuania
M.J. Bilinskas, I. Grigelionis, M. Janulis, D. Martisiute, P. Petrov, T. Sabonis

Centro de Investigacion y de Estudios Avanzados del IPN, Mexico City, Mexico
H. Castilla-Valdez, E. De La Cruz-Burelo, I. Heredia-de La Cruz, R. Lopez-Fernandez, R. Magaña Villalba, A. Sánchez-Hernández, L.M. Villaseñor-Cendejas

Universidad Iberoamericana, Mexico City, Mexico
S. Carrillo Moreno, F. Vazquez Valencia

Benemerita Universidad Autonoma de Puebla, Puebla, Mexico
H.A. Salazar Ibarguen

Universidad Autónoma de San Luis Potosí, San Luis Potosí, Mexico
E. Casimiro Linares, A. Morelos Pineda, M.A. Reyes-Santos

University of Auckland, Auckland, New Zealand
D. Krofcheck, J. Tam

University of Canterbury, Christchurch, New Zealand
P.H. Butler, R. Doesburg, H. Silverwood

National Centre for Physics, Quaid-I-Azam University, Islamabad, Pakistan
M. Ahmad, I. Ahmed, M.I. Asghar, H.R. Hoorani, W.A. Khan, T. Khurshid, S. Qazi

Institute of Experimental Physics, Faculty of Physics, University of Warsaw, Warsaw, Poland
G. Brona, M. Cwiok, W. Dominik, K. Doroba, A. Kalinowski, M. Konecki, J. Krolikowski

Soltan Institute for Nuclear Studies, Warsaw, Poland
T. Frueboes, R. Gokieli, M. Górski, M. Kazana, K. Nawrocki, K. Romanowska-Rybinska, M. Szleper, G. Wrochna, P. Zalewski

Laboratório de Instrumentação e Física Experimental de Partículas, Lisboa, Portugal
N. Almeida, P. Bargassa, A. David, P. Faccioli, P.G. Ferreira Parracho, M. Gallinaro, P. Musella, A. Nayak, P.Q. Ribeiro, J. Seixas, J. Varela

Joint Institute for Nuclear Research, Dubna, Russia
S. Afanasiev, I. Belotelov, P. Bunin, I. Golutvin, A. Kamenev, V. Karjavin, G. Kozlov, A. Lanev, P. Moisenz, V. Palichik, V. Perelygin, S. Shmatov, V. Smirnov, A. Volodko, A. Zarubin

Petersburg Nuclear Physics Institute, Gatchina (St Petersburg), Russia
V. Golovtsov, Y. Ivanov, V. Kim, P. Levchenko, V. Murzin, V. Oreshkin, I. Smirnov, V. Sulimov, L. Uvarov, S. Vavilov, A. Vorobyev, An. Vorobyev

Institute for Nuclear Research, Moscow, Russia
Yu. Andreev, A. Dermenev, S. Gninenko, N. Golubev, M. Kirsanov, N. Krasnikov, V. Matveev, A. Pashenkov, A. Toropin, S. Troitsky

Institute for Theoretical and Experimental Physics, Moscow, Russia
V. Epshteyn, V. Gavrilov, V. Kaftanov[†], M. Kossov[1], A. Krokhotin, N. Lychkovskaya, V. Popov, G. Safronov, S. Semenov, V. Stolin, E. Vlasov, A. Zhokin

Moscow State University, Moscow, Russia
E. Boos, M. Dubinin[23], L. Dudko, A. Ershov, A. Gribushin, O. Kodolova, I. Lokhtin, A. Markina, S. Obraztsov, M. Perfilov, S. Petrushanko, L. Sarycheva, V. Savrin, A. Snigirev

P.N. Lebedev Physical Institute, Moscow, Russia
V. Andreev, M. Azarkin, I. Dremin, M. Kirakosyan, A. Leonidov, S.V. Rusakov, A. Vinogradov

State Research Center of Russian Federation, Institute for High Energy Physics, Protvino, Russia
I. Azhgirey, S. Bitioukov, V. Grishin[1], V. Kachanov, D. Konstantinov, A. Korablev, V. Krychkine, V. Petrov, R. Ryutin, S. Slabospitsky, A. Sobol, L. Tourtchanovitch, S. Troshin, N. Tyurin, A. Uzunian, A. Volkov

University of Belgrade, Faculty of Physics and Vinca Institute of Nuclear Sciences, Belgrade, Serbia
P. Adzic[24], M. Djordjevic, D. Krpic[24], J. Milosevic

Centro de Investigaciones Energéticas Medioambientales y Tecnológicas (CIEMAT), Madrid, Spain
M. Aguilar-Benitez, J. Alcaraz Maestre, P. Arce, C. Battilana, E. Calvo, M. Cepeda, M. Cerrada, M. Chamizo Llatas, N. Colino, B. De La Cruz, A. Delgado Peris, C. Diez Pardos, D. Domínguez, C. Fernandez Bedoya, J.P. Fernández Ramos, A. Ferrando, J. Flix, M.C. Fouz, P. Garcia-Abia, O. Gonzalez Lopez, S. Goy Lopez, J.M. Hernandez, M.I. Josa, G. Merino, J. Puerta Pelayo, I. Redondo, L. Romero, J. Santaolalla, M.S. Soares, C. Willmott

Universidad Autónoma de Madrid, Madrid, Spain
C. Albajar, G. Codispoti, J.F. de Trocóniz

Universidad de Oviedo, Oviedo, Spain
J. Cuevas, J. Fernandez Menendez, S. Folgueras, I. Gonzalez Caballero, L. Lloret Iglesias, J.M. Vizan Garcia

Instituto de Física de Cantabria (IFCA), CSIC-Universidad de Cantabria, Santander, Spain
J.A. Brochero Cifuentes, I.J. Cabrillo, A. Calderon, S.H. Chuang, J. Duarte Campderros, M. Felcini[25], M. Fernandez, G. Gomez, J. Gonzalez Sanchez, C. Jorda, P. Lobelle Pardo, A. Lopez Virto, J. Marco, R. Marco, C. Martinez Rivero, F. Matorras, F.J. Munoz Sanchez, J. Piedra Gomez[26], T. Rodrigo, A.Y. Rodriguez-Marrero, A. Ruiz Jimeno, L. Scodellaro, M. Sobron Sanudo, I. Vila, R. Vilar Cortabitarte

CERN, European Organization for Nuclear Research, Geneva, Switzerland
D. Abbaneo, E. Auffray, G. Auzinger, P. Baillon, A.H. Ball, D. Barney, A.J. Bell[27], D. Benedetti, C. Bernet[3], W. Bialas, P. Bloch, A. Bocci, S. Bolognesi, M. Bona, H. Breuker, K. Bunkowski, T. Camporesi, G. Cerminara, T. Christiansen, J.A. Coarasa Perez, B. Curé, D. D'Enterria, A. De Roeck, S. Di Guida, N. Dupont-Sagorin, A. Elliott-Peisert, B. Frisch, W. Funk, A. Gaddi, G. Georgiou, H. Gerwig, D. Gigi, K. Gill, D. Giordano, F. Glege, R. Gomez-Reino Garrido, M. Gouzevitch, P. Govoni, S. Gowdy, L. Guiducci, M. Hansen, C. Hartl, J. Harvey, J. Hegeman, B. Hegner, H.F. Hoffmann, A. Honma, V. Innocente, P. Janot, K. Kaadze, E. Karavakis, P. Lecoq, C. Lourenço, T. Mäki, M. Malberti, L. Malgeri, M. Mannelli, L. Masetti, A. Maurisset, F. Meijers, S. Mersi, E. Meschi, R. Moser, M.U. Mozer, M. Mulders, E. Nesvold[1], M. Nguyen, T. Orimoto, L. Orsini, E. Palencia Cortezon, E. Perez, A. Petrilli, A. Pfeiffer, M. Pierini, M. Pimiä, D. Piparo, G. Polese, A. Racz, J. Rodrigues Antunes, G. Rolandi[28], T. Rommerskirchen, M. Rovere, H. Sakulin, C. Schäfer, C. Schwick, I. Segoni, A. Sharma, P. Siegrist, M. Simon, P. Sphicas[29], M. Spiropulu[23], M. Stoye, M. Tadel, P. Tropea, A. Tsirou, P. Vichoudis, M. Voutilainen, W.D. Zeuner

Paul Scherrer Institut, Villigen, Switzerland
W. Bertl, K. Deiters, W. Erdmann, K. Gabathuler, R. Horisberger, Q. Ingram, H.C. Kaestli, S. König, D. Kotlinski, U. Langenegger, F. Meier, D. Renker, T. Rohe, J. Sibille[30], A. Starodumov[31]

Institute for Particle Physics, ETH Zurich, Zurich, Switzerland
L. Bäni, P. Bortignon, L. Caminada[32], N. Chanon, Z. Chen, S. Cittolin, G. Dissertori, M. Dittmar, J. Eugster, K. Freudenreich, C. Grab, W. Hintz, P. Lecomte, W. Lustermann, C. Marchica[32], P. Martinez Ruiz del Arbol, P. Meridiani, P. Milenovic[33], F. Moortgat, C. Nägeli[32], P. Nef, F. Nessi-Tedaldi, L. Pape, F. Pauss, T. Punz, A. Rizzi, F.J. Ronga, M. Rossini, L. Sala, A.K. Sanchez, M.-C. Sawley, B. Stieger, L. Tauscher[†], A. Thea, K. Theofilatos, D. Treille, C. Urscheler, R. Wallny, M. Weber, L. Wehrli, J. Weng

Universität Zürich, Zurich, Switzerland
E. Aguilo, C. Amsler, V. Chiochia, S. De Visscher, C. Favaro, M. Ivova Rikova, B. Millan Mejias, P. Otiougova, C. Regenfus, P. Robmann, A. Schmidt, H. Snoek

National Central University, Chung-Li, Taiwan
Y.H. Chang, K.H. Chen, C.M. Kuo, S.W. Li, W. Lin, Z.K. Liu, Y.J. Lu, D. Mekterovic, R. Volpe, J.H. Wu, S.S. Yu

National Taiwan University (NTU), Taipei, Taiwan
P. Bartalini, P. Chang, Y.H. Chang, Y.W. Chang, Y. Chao, K.F. Chen, W.-S. Hou, Y. Hsiung, K.Y. Kao, Y.J. Lei, R.-S. Lu, J.G. Shiu, Y.M. Tzeng, M. Wang

Cukurova University, Adana, Turkey
A. Adiguzel, M.N. Bakirci[34], S. Cerci[35], C. Dozen, I. Dumanoglu, E. Eskut, S. Girgis, G. Gokbulut, I. Hos, E.E. Kangal, A. Kayis Topaksu, G. Önengüt, K. Ozdemir, S. Ozturk[36], A. Polatoz, K. Sogut[37], D. Sunar Cerci[35], B. Tali[35], H. Topakli[34], D. Uzun, L.N. Vergili, M. Vergili

Middle East Technical University, Physics Department, Ankara, Turkey
I.V. Akin, T. Aliev, B. Bilin, S. Bilmis, M. Deniz, H. Gamsizkan, A.M. Guler, K. Ocalan, A. Ozpineci, M. Serin, R. Sever, U.E. Surat, E. Yildirim, M. Zeyrek

Bogazici University, Istanbul, Turkey
M. Deliomeroglu, D. Demir[38], E. Gülmez, B. Isildak, M. Kaya[39], O. Kaya[39], M. Özbek, S. Ozkorucuklu[40], N. Sonmez[41]

National Scientific Center, Kharkov Institute of Physics and Technology, Kharkov, Ukraine
L. Levchuk

University of Bristol, Bristol, UK
F. Bostock, J.J. Brooke, T.L. Cheng, E. Clement, D. Cussans, R. Frazier, J. Goldstein, M. Grimes, M. Hansen, D. Hartley, G.P. Heath, H.F. Heath, L. Kreczko, S. Metson, D.M. Newbold[42], K. Nirunpong, A. Poll, S. Senkin, V.J. Smith, S. Ward

Rutherford Appleton Laboratory, Didcot, UK
L. Basso[43], K.W. Bell, A. Belyaev[43], C. Brew, R.M. Brown, B. Camanzi, D.J.A. Cockerill, J.A. Coughlan, K. Harder, S. Harper, J. Jackson, B.W. Kennedy, E. Olaiya, D. Petyt, B.C. Radburn-Smith, C.H. Shepherd-Themistocleous, I.R. Tomalin, W.J. Womersley, S.D. Worm

Imperial College, London, UK
R. Bainbridge, G. Ball, J. Ballin, R. Beuselinck, O. Buchmuller, D. Colling, N. Cripps, M. Cutajar, G. Davies, M. Della Negra, W. Ferguson, J. Fulcher, D. Futyan, A. Gilbert, A. Guneratne Bryer, G. Hall, Z. Hatherell, J. Hays, G. Iles, M. Jarvis, G. Karapostoli, L. Lyons, B.C. MacEvoy, A.-M. Magnan, J. Marrouche, B. Mathias, R. Nandi, J. Nash, A. Nikitenko[31], A. Papageorgiou, M. Pesaresi, K. Petridis, M. Pioppi[44], D.M. Raymond, S. Rogerson, N. Rompotis, A. Rose, M.J. Ryan, C. Seez, P. Sharp, A. Sparrow, A. Tapper, S. Tourneur, M. Vazquez Acosta, T. Virdee, S. Wakefield, N. Wardle, D. Wardrope, T. Whyntie

Brunel University, Uxbridge, UK
M. Barrett, M. Chadwick, J.E. Cole, P.R. Hobson, A. Khan, P. Kyberd, D. Leslie, W. Martin, I.D. Reid, L. Teodorescu

Baylor University, Waco, USA
K. Hatakeyama, H. Liu

Boston University, Boston, USA
T. Bose, E. Carrera Jarrin, C. Fantasia, A. Heister, J. St. John, P. Lawson, D. Lazic, J. Rohlf, D. Sperka, L. Sulak

Brown University, Providence, USA
A. Avetisyan, S. Bhattacharya, J.P. Chou, D. Cutts, A. Ferapontov, U. Heintz, S. Jabeen, G. Kukartsev, G. Landsberg, M. Luk, M. Narain, D. Nguyen, M. Segala, T. Sinthuprasith, T. Speer, K.V. Tsang

University of California, Davis, Davis, USA
R. Breedon, M. Calderon De La Barca Sanchez, S. Chauhan, M. Chertok, J. Conway, P.T. Cox, J. Dolen, R. Erbacher, E. Friis, W. Ko, A. Kopecky, R. Lander, H. Liu, S. Maruyama, T. Miceli, M. Nikolic, D. Pellett, J. Robles, S. Salur, T. Schwarz, M. Searle, J. Smith, M. Squires, M. Tripathi, R. Vasquez Sierra, C. Veelken

University of California, Los Angeles, Los Angeles, USA
V. Andreev, K. Arisaka, D. Cline, R. Cousins, A. Deisher, J. Duris, S. Erhan, C. Farrell, J. Hauser, M. Ignatenko, C. Jarvis, C. Plager, G. Rakness, P. Schlein[†], J. Tucker, V. Valuev

University of California, Riverside, Riverside, USA
J. Babb, A. Chandra, R. Clare, J. Ellison, J.W. Gary, F. Giordano, G. Hanson, G.Y. Jeng, S.C. Kao, F. Liu, H. Liu, O.R. Long, A. Luthra, H. Nguyen, B.C. Shen[†], R. Stringer, J. Sturdy, S. Sumowidagdo, R. Wilken, S. Wimpenny

University of California, San Diego, La Jolla, USA
W. Andrews, J.G. Branson, G.B. Cerati, D. Evans, F. Golf, A. Holzner, R. Kelley, M. Lebourgeois, J. Letts, B. Mangano, S. Padhi, C. Palmer, G. Petrucciani, H. Pi, M. Pieri, R. Ranieri, M. Sani, V. Sharma, S. Simon, E. Sudano, Y. Tu, A. Vartak, S. Wasserbaech[45], F. Würthwein, A. Yagil, J. Yoo

University of California, Santa Barbara, Santa Barbara, USA
D. Barge, R. Bellan, C. Campagnari, M. D'Alfonso, T. Danielson, K. Flowers, P. Geffert, J. Incandela, C. Justus, P. Kalavase, S.A. Koay, D. Kovalskyi, V. Krutelyov, S. Lowette, N. Mccoll, V. Pavlunin, F. Rebassoo, J. Ribnik, J. Richman, R. Rossin, D. Stuart, W. To, J.R. Vlimant

California Institute of Technology, Pasadena, USA
A. Apresyan, A. Bornheim, J. Bunn, Y. Chen, M. Gataullin, Y. Ma, A. Mott, H.B. Newman, C. Rogan, K. Shin, V. Timciuc, P. Traczyk, J. Veverka, R. Wilkinson, Y. Yang, R.Y. Zhu

Carnegie Mellon University, Pittsburgh, USA
B. Akgun, R. Carroll, T. Ferguson, Y. Iiyama, D.W. Jang, S.Y. Jun, Y.F. Liu, M. Paulini, J. Russ, H. Vogel, I. Vorobiev

University of Colorado at Boulder, Boulder, USA
J.P. Cumalat, M.E. Dinardo, B.R. Drell, C.J. Edelmaier, W.T. Ford, A. Gaz, B. Heyburn, E. Luiggi Lopez, U. Nauenberg, J.G. Smith, K. Stenson, K.A. Ulmer, S.R. Wagner, S.L. Zang

Cornell University, Ithaca, USA
L. Agostino, J. Alexander, D. Cassel, A. Chatterjee, S. Das, N. Eggert, L.K. Gibbons, B. Heltsley, W. Hopkins, A. Khukhunaishvili, B. Kreis, G. Nicolas Kaufman, J.R. Patterson, D. Puigh, A. Ryd, E. Salvati, X. Shi, W. Sun, W.D. Teo, J. Thom, J. Thompson, J. Vaughan, Y. Weng, L. Winstrom, P. Wittich

Fairfield University, Fairfield, USA
A. Biselli, G. Cirino, D. Winn

Fermi National Accelerator Laboratory, Batavia, USA
S. Abdullin, M. Albrow, J. Anderson, G. Apollinari, M. Atac, J.A. Bakken, S. Banerjee, L.A.T. Bauerdick, A. Beretvas, J. Berryhill, P.C. Bhat, I. Bloch, F. Borcherding, K. Burkett, J.N. Butler, V. Chetluru, H.W.K. Cheung, F. Chlebana, S. Cihangir, W. Cooper, D.P. Eartly, V.D. Elvira, S. Esen, I. Fisk, J. Freeman, Y. Gao, E. Gottschalk, D. Green, K. Gunthoti, O. Gutsche, J. Hanlon, R.M. Harris, J. Hirschauer, B. Hooberman, H. Jensen, M. Johnson, U. Joshi, R. Khatiwada, B. Klima, K. Kousouris, S. Kunori, S. Kwan, C. Leonidopoulos, P. Limon, D. Lincoln, R. Lipton, J. Lykken, K. Maeshima, J.M. Marraffino, D. Mason, P. McBride, T. Miao, K. Mishra, S. Mrenna, Y. Musienko[46], C. Newman-Holmes, V. O'Dell, R. Pordes, O. Prokofyev, N. Saoulidou, E. Sexton-Kennedy, S. Sharma, W.J. Spalding, L. Spiegel, P. Tan, L. Taylor, S. Tkaczyk, L. Uplegger, E.W. Vaandering, R. Vidal, J. Whitmore, W. Wu, F. Yang, F. Yumiceva, J.C. Yun

University of Florida, Gainesville, USA
D. Acosta, P. Avery, D. Bourilkov, M. Chen, M. De Gruttola, G.P. Di Giovanni, D. Dobur, A. Drozdetskiy, R.D. Field, M. Fisher, Y. Fu, I.K. Furic, J. Gartner, B. Kim, J. Konigsberg, A. Korytov, A. Kropivnitskaya, T. Kypreos, K. Matchev, G. Mitselmakher, L. Muniz, C. Prescott, R. Remington, M. Schmitt, B. Scurlock, P. Sellers, N. Skhirtladze, M. Snowball, D. Wang, J. Yelton, M. Zakaria

Florida International University, Miami, USA
C. Ceron, V. Gaultney, L. Kramer, L.M. Lebolo, S. Linn, P. Markowitz, G. Martinez, D. Mesa, J.L. Rodriguez

Florida State University, Tallahassee, USA
T. Adams, A. Askew, J. Bochenek, J. Chen, B. Diamond, S.V. Gleyzer, J. Haas, S. Hagopian, V. Hagopian, M. Jenkins, K.F. Johnson, H. Prosper, L. Quertenmont, S. Sekmen, V. Veeraraghavan

Florida Institute of Technology, Melbourne, USA
M.M. Baarmand, B. Dorney, S. Guragain, M. Hohlmann, H. Kalakhety, R. Ralich, I. Vodopiyanov

University of Illinois at Chicago (UIC), Chicago, USA
M.R. Adams, I.M. Anghel, L. Apanasevich, Y. Bai, V.E. Bazterra, R.R. Betts, J. Callner, R. Cavanaugh, C. Dragoiu, L. Gauthier, C.E. Gerber, S. Hamdan, D.J. Hofman, S. Khalatyan, G.J. Kunde[47], F. Lacroix, M. Malek, C. O'Brien, C. Silvestre, A. Smoron, D. Strom, N. Varelas

The University of Iowa, Iowa City, USA
U. Akgun, E.A. Albayrak, B. Bilki, W. Clarida, F. Duru, C.K. Lae, E. McCliment, J.-P. Merlo, H. Mermerkaya[48], A. Mestvirishvili, A. Moeller, J. Nachtman, C.R. Newsom, E. Norbeck, J. Olson, Y. Onel, F. Ozok, S. Sen, J. Wetzel, T. Yetkin, K. Yi

Johns Hopkins University, Baltimore, USA
B.A. Barnett, B. Blumenfeld, A. Bonato, C. Eskew, D. Fehling, G. Giurgiu, A.V. Gritsan, Z.J. Guo, G. Hu, P. Maksimovic, S. Rappoccio, M. Swartz, N.V. Tran, A. Whitbeck

The University of Kansas, Lawrence, USA
P. Baringer, A. Bean, G. Benelli, O. Grachov, R.P. Kenny Iii, M. Murray, D. Noonan, S. Sanders, J.S. Wood, V. Zhukova

Kansas State University, Manhattan, USA
A.F. Barfuss, T. Bolton, I. Chakaberia, A. Ivanov, S. Khalil, M. Makouski, Y. Maravin, S. Shrestha, I. Svintradze, Z. Wan

Lawrence Livermore National Laboratory, Livermore, USA
J. Gronberg, D. Lange, D. Wright

University of Maryland, College Park, USA
A. Baden, M. Boutemeur, S.C. Eno, D. Ferencek, J.A. Gomez, N.J. Hadley, R.G. Kellogg, M. Kirn, Y. Lu, A.C. Mignerey, K. Rossato, P. Rumerio, F. Santanastasio, A. Skuja, J. Temple, M.B. Tonjes, S.C. Tonwar, E. Twedt

Massachusetts Institute of Technology, Cambridge, USA
B. Alver, G. Bauer, J. Bendavid, W. Busza, E. Butz, I.A. Cali, M. Chan, V. Dutta, P. Everaerts, G. Gomez Ceballos, M. Goncharov, K.A. Hahn, P. Harris, Y. Kim, M. Klute, Y.-J. Lee, W. Li, C. Loizides, P.D. Luckey, T. Ma, S. Nahn, C. Paus, D. Ralph, C. Roland, G. Roland, M. Rudolph, G.S.F. Stephans, F. Stöckli, K. Sumorok, K. Sung, E.A. Wenger, S. Xie, M. Yang, Y. Yilmaz, A.S. Yoon, M. Zanetti

University of Minnesota, Minneapolis, USA
S.I. Cooper, P. Cushman, B. Dahmes, A. De Benedetti, P.R. Dudero, G. Franzoni, J. Haupt, K. Klapoetke, Y. Kubota, J. Mans, V. Rekovic, R. Rusack, M. Sasseville, A. Singovsky, N. Tambe

University of Mississippi, University, USA
L.M. Cremaldi, R. Godang, R. Kroeger, L. Perera, R. Rahmat, D.A. Sanders, D. Summers

University of Nebraska-Lincoln, Lincoln, USA
K. Bloom, S. Bose, J. Butt, D.R. Claes, A. Dominguez, M. Eads, J. Keller, T. Kelly, I. Kravchenko, J. Lazo-Flores, H. Malbouisson, S. Malik, G.R. Snow

State University of New York at Buffalo, Buffalo, USA
U. Baur, A. Godshalk, I. Iashvili, S. Jain, A. Kharchilava, A. Kumar, S.P. Shipkowski, K. Smith

Northeastern University, Boston, USA
G. Alverson, E. Barberis, D. Baumgartel, O. Boeriu, M. Chasco, S. Reucroft, J. Swain, D. Trocino, D. Wood, J. Zhang

Northwestern University, Evanston, USA
A. Anastassov, A. Kubik, N. Odell, R.A. Ofierzynski, B. Pollack, A. Pozdnyakov, M. Schmitt, S. Stoynev, M. Velasco, S. Won

University of Notre Dame, Notre Dame, USA
L. Antonelli, D. Berry, A. Brinkerhoff, M. Hildreth, C. Jessop, D.J. Karmgard, J. Kolb, T. Kolberg, K. Lannon, W. Luo, S. Lynch, N. Marinelli, D.M. Morse, T. Pearson, R. Ruchti, J. Slaunwhite, N. Valls, M. Wayne, J. Ziegler

The Ohio State University, Columbus, USA
B. Bylsma, L.S. Durkin, J. Gu, C. Hill, P. Killewald, K. Kotov, T.Y. Ling, M. Rodenburg, G. Williams

Princeton University, Princeton, USA
N. Adam, E. Berry, P. Elmer, D. Gerbaudo, V. Halyo, P. Hebda, A. Hunt, J. Jones, E. Laird, D. Lopes Pegna, D. Marlow, T. Medvedeva, M. Mooney, J. Olsen, P. Piroué, X. Quan, H. Saka, D. Stickland, C. Tully, J.S. Werner, A. Zuranski

University of Puerto Rico, Mayaguez, USA
J.G. Acosta, X.T. Huang, A. Lopez, H. Mendez, S. Oliveros, J.E. Ramirez Vargas, A. Zatserklyaniy

Purdue University, West Lafayette, USA
E. Alagoz, V.E. Barnes, G. Bolla, L. Borrello, D. Bortoletto, A. Everett, A.F. Garfinkel, L. Gutay, Z. Hu, M. Jones, O. Koybasi, M. Kress, A.T. Laasanen, N. Leonardo, C. Liu, V. Maroussov, P. Merkel, D.H. Miller, N. Neumeister, I. Shipsey, D. Silvers, A. Svyatkovskiy, H.D. Yoo, J. Zablocki, Y. Zheng

Purdue University Calumet, Hammond, USA
P. Jindal, N. Parashar

Rice University, Houston, USA
C. Boulahouache, V. Cuplov, K.M. Ecklund, F.J.M. Geurts, B.P. Padley, R. Redjimi, J. Roberts, J. Zabel

University of Rochester, Rochester, USA
B. Betchart, A. Bodek, Y.S. Chung, R. Covarelli, P. de Barbaro, R. Demina, Y. Eshaq, H. Flacher, A. Garcia-Bellido, P. Goldenzweig, Y. Gotra, J. Han, A. Harel, D.C. Miner, D. Orbaker, G. Petrillo, D. Vishnevskiy, M. Zielinski

The Rockefeller University, New York, USA
A. Bhatti, R. Ciesielski, L. Demortier, K. Goulianos, G. Lungu, S. Malik, C. Mesropian, M. Yan

Rutgers, the State University of New Jersey, Piscataway, USA
O. Atramentov, A. Barker, D. Duggan, Y. Gershtein, R. Gray, E. Halkiadakis, D. Hidas, D. Hits, A. Lath, S. Panwalkar, R. Patel, A. Richards, K. Rose, S. Schnetzer, S. Somalwar, R. Stone, S. Thomas

University of Tennessee, Knoxville, USA
G. Cerizza, M. Hollingsworth, S. Spanier, Z.C. Yang, A. York

Texas A&M University, College Station, USA
R. Eusebi, W. Flanagan, J. Gilmore, A. Gurrola, T. Kamon, V. Khotilovich, R. Montalvo, I. Osipenkov, Y. Pakhotin, J. Pivarski, A. Safonov, S. Sengupta, A. Tatarinov, D. Toback, M. Weinberger

Texas Tech University, Lubbock, USA
N. Akchurin, C. Bardak, J. Damgov, C. Jeong, K. Kovitanggoon, S.W. Lee, P. Mane, Y. Roh, A. Sill, I. Volobouev, R. Wigmans, E. Yazgan

Vanderbilt University, Nashville, USA
E. Appelt, E. Brownson, D. Engh, C. Florez, W. Gabella, M. Issah, W. Johns, P. Kurt, C. Maguire, A. Melo, P. Sheldon, B. Snook, S. Tuo, J. Velkovska

University of Virginia, Charlottesville, USA
M.W. Arenton, M. Balazs, S. Boutle, B. Cox, B. Francis, R. Hirosky, A. Ledovskoy, C. Lin, C. Neu, R. Yohay

Wayne State University, Detroit, USA
S. Gollapinni, R. Harr, P.E. Karchin, P. Lamichhane, M. Mattson, C. Milstène, A. Sakharov

University of Wisconsin, Madison, USA
M. Anderson, M. Bachtis, J.N. Bellinger, D. Carlsmith, S. Dasu, J. Efron, K. Flood, L. Gray, K.S. Grogg, M. Grothe, R. Hall-Wilton, M. Herndon, A. Hervé, P. Klabbers, J. Klukas, A. Lanaro, C. Lazaridis, J. Leonard, R. Loveless, A. Mohapatra, F. Palmonari, D. Reeder, I. Ross, A. Savin, W.H. Smith, J. Swanson, M. Weinberg

†: Deceased
1: Also at CERN, European Organization for Nuclear Research, Geneva, Switzerland
2: Also at Universidade Federal do ABC, Santo Andre, Brazil
3: Also at Laboratoire Leprince-Ringuet, Ecole Polytechnique, IN2P3-CNRS, Palaiseau, France
4: Also at Suez Canal University, Suez, Egypt
5: Also at British University, Cairo, Egypt
6: Also at Fayoum University, El-Fayoum, Egypt
7: Also at Soltan Institute for Nuclear Studies, Warsaw, Poland
8: Also at Massachusetts Institute of Technology, Cambridge, USA
9: Also at Université de Haute-Alsace, Mulhouse, France
10: Also at Brandenburg University of Technology, Cottbus, Germany
11: Also at Moscow State University, Moscow, Russia
12: Also at Institute of Nuclear Research ATOMKI, Debrecen, Hungary
13: Also at Eötvös Loránd University, Budapest, Hungary
14: Also at Tata Institute of Fundamental Research—HECR, Mumbai, India
15: Also at University of Visva-Bharati, Santiniketan, India
16: Also at Sharif University of Technology, Tehran, Iran
17: Also at Shiraz University, Shiraz, Iran
18: Also at Isfahan University of Technology, Isfahan, Iran
19: Also at Facolta' Ingegneria Università di Roma "La Sapienza", Roma, Italy
20: Also at Università della Basilicata, Potenza, Italy
21: Also at Laboratori Nazionali di Legnaro dell'INFN, Legnaro, Italy
22: Also at Università degli studi di Siena, Siena, Italy
23: Also at California Institute of Technology, Pasadena, USA
24: Also at Faculty of Physics of University of Belgrade, Belgrade, Serbia
25: Also at University of California, Los Angeles, Los Angeles, USA
26: Also at University of Florida, Gainesville, USA

27: Also at Université de Genève, Geneva, Switzerland
28: Also at Scuola Normale e Sezione dell'INFN, Pisa, Italy
29: Also at University of Athens, Athens, Greece
30: Also at The University of Kansas, Lawrence, USA
31: Also at Institute for Theoretical and Experimental Physics, Moscow, Russia
32: Also at Paul Scherrer Institut, Villigen, Switzerland
33: Also at University of Belgrade, Faculty of Physics and Vinca Institute of Nuclear Sciences, Belgrade, Serbia
34: Also at Gaziosmanpasa University, Tokat, Turkey
35: Also at Adiyaman University, Adiyaman, Turkey
36: Also at The University of Iowa, Iowa City, USA
37: Also at Mersin University, Mersin, Turkey
38: Also at Izmir Institute of Technology, Izmir, Turkey
39: Also at Kafkas University, Kars, Turkey
40: Also at Suleyman Demirel University, Isparta, Turkey
41: Also at Ege University, Izmir, Turkey
42: Also at Rutherford Appleton Laboratory, Didcot, UK
43: Also at School of Physics and Astronomy, University of Southampton, Southampton, UK
44: Also at INFN Sezione di Perugia; Università di Perugia, Perugia, Italy
45: Also at Utah Valley University, Orem, USA
46: Also at Institute for Nuclear Research, Moscow, Russia
47: Also at Los Alamos National Laboratory, Los Alamos, USA
48: Also at Erzincan University, Erzincan, Turkey